

# 博士學位論文

進展型小細胞肺癌における腫瘍微小免疫環境と  
フレームシフト変異由来ネオアンチゲンの  
PD-L1 阻害薬の効果との関連

近畿大学大学院  
医学研究科医学系専攻  
金 村 宙 昌

Doctoral Dissertation

**The Tumor Immune Microenvironment and Frameshift  
Neoantigen Load Determine Response to PD-L1  
Blockade in Extensive-Stage SCLC**

November 2022

Major in Medical Sciences  
Kindai University Graduate School of Medical Sciences

**Hiroaki Kanemura**

## 同意書

2022年11月9日

近畿大学大学院  
医学研究科長 殿共著者 林秀敏 共著者 谷崎潤子 共著者 鈴木真一郎 共著者 川中雄介 共著者 原谷浩司 共著者 高濱隆幸 共著者 \_\_\_\_\_ 共著者 \_\_\_\_\_ 共著者 \_\_\_\_\_ 共著者 \_\_\_\_\_ 

## 論文題目

The Tumor Immune Microenvironment and Frameshift Neoantigen Load  
Determine Response to PD-L1 Blockade in Extensive-Stage SCLC

下記の博士論文提出者が、標記論文を貴学医学博士の学位論文（主論文）  
として使用することに同意いたします。

また、標記論文を再び学位論文として使用しないことを誓約いたします。

## 記

1. 博士論文提出者氏名

金村宙昌

2. 専攻分野 医学系

腫瘍病態制御学

同意書

2022年11月9日

近畿大学大学院  
医学研究科長 殿

共著者 西尾和人 

共著者 坂井千子 

共著者 \_\_\_\_\_ (印)

論文題目

The Tumor Immune Microenvironment and Frameshift Neoantigen Load Determine Response to PD-L1 Blockade in Extensive-Stage SCLC

下記の博士論文提出者が、標記論文を貴学医学博士の学位論文（主論文）として使用することに同意いたします。

また、標記論文を再び学位論文として使用しないことを誓約いたします。

記

1. 博士論文提出者氏名

金村宙昌

2. 専攻分野 医学系

腫瘍病態制御学

## 同意書

2022年11月9日

近畿大学大学院  
医学研究科長 殿

共著者	中川和彦 	共著者	_____ 
共著者	_____ 	共著者	_____ 
共著者	_____ 	共著者	_____ 
共著者	_____ 	共著者	_____ 
共著者	_____ 	共著者	_____ 

## 論文題目

The Tumor Immune Microenvironment and Frameshift Neoantigen Load Determine Response to PD-L1 Blockade in Extensive-Stage SCLC

下記の博士論文提出者が、標記論文を貴学医学博士の学位論文（主論文）として使用することに同意いたします。

また、標記論文を再び学位論文として使用しないことを誓約いたします。

## 記

- |              |         |
|--------------|---------|
| 1. 博士論文提出者氏名 | 金村宙昌    |
| 2. 専攻分野 医学系  | 腫瘍病態制御学 |

同意書

2022 年 11 月 9 日

近畿大学大学院  
医学研究科長 殿

共著者	<u>千原 康敬</u>		共著者	_____	Ⓔ
共著者	_____	Ⓔ	共著者	_____	Ⓔ
共著者	_____	Ⓔ	共著者	_____	Ⓔ
共著者	_____	Ⓔ	共著者	_____	Ⓔ
共著者	_____	Ⓔ	共著者	_____	Ⓔ

論文題目

The Tumor Immune Microenvironment and Frameshift Neoantigen Load Determine Response to PD-L1 Blockade in Extensive-Stage SCLC

下記の博士論文提出者が、標記論文を貴学医学博士の学位論文（主論文）として使用することに同意いたします。

また、標記論文を再び学位論文として使用しないことを誓約いたします。

記

1. 博士論文提出者氏名

金村宙昌

2. 専攻分野 医学系

腫瘍病態制御学

同意書

2022 年 11 月 9 日

近畿大学大学院  
医学研究科長 殿

共著者 伊藤 彰彦 

共著者 大谷 知之 

共著者 \_\_\_\_\_ 

共著者 \_\_\_\_\_ 

共著者 \_\_\_\_\_ 

共著者 \_\_\_\_\_ 

共著者 \_\_\_\_\_ 

共著者 \_\_\_\_\_ 

共著者 \_\_\_\_\_ 

共著者 \_\_\_\_\_ 

論文題目

The Tumor Immune Microenvironment and Frameshift Neoantigen Load Determine Response to PD-L1 Blockade in Extensive-Stage SCLC

下記の博士論文提出者が、標記論文を貴学医学博士の学位論文（主論文）として使用することに同意いたします。

また、標記論文を再び学位論文として使用しないことを誓約いたします。

記

1. 博士論文提出者氏名

金村宙昌

2. 専攻分野 医学系

腫瘍病態制御学

同意書

2022 年 11 月 9 日

近畿大学大学院  
医学研究科長 殿

共著者	今井 亮介		共著者	_____	Ⓔ
共著者	_____	Ⓔ	共著者	_____	Ⓔ
共著者	_____	Ⓔ	共著者	_____	Ⓔ
共著者	_____	Ⓔ	共著者	_____	Ⓔ
共著者	_____	Ⓔ	共著者	_____	Ⓔ

論文題目

The Tumor Immune Microenvironment and Frameshift Neoantigen Load Determine Response to PD-L1 Blockade in Extensive-Stage SCLC

下記の博士論文提出者が、標記論文を貴学医学博士の学位論文（主論文）として使用することに同意いたします。

また、標記論文を再び学位論文として使用しないことを誓約いたします。

記

- |              |         |
|--------------|---------|
| 1. 博士論文提出者氏名 | 金村宙昌    |
| 2. 専攻分野 医学系  | 腫瘍病態制御学 |

同意書

2022年 11月 9日

近畿大学大学院  
医学研究科長 殿

共著者 工藤 慶太 

共著者 金田 裕靖 

共著者 津谷 あす香 

共著者 福田 泰 

共著者 富田 秀太 

共著者 \_\_\_\_\_ 

共著者 \_\_\_\_\_ 

共著者 \_\_\_\_\_ 

共著者 \_\_\_\_\_ 

共著者 \_\_\_\_\_ 

論文題目

The Tumor Immune Microenvironment and Frameshift Neoantigen Load Determine Response to PD-L1 Blockade in Extensive-Stage SCLC

下記の博士論文提出者が、標記論文を貴学医学博士の学位論文（主論文）として使用することに同意いたします。

また、標記論文を再び学位論文として使用しないことを誓約いたします。

記

1. 博士論文提出者氏名

金村宙昌

2. 専攻分野 医学系

腫瘍病態制御学

## The Tumor Immune Microenvironment and Frameshift Neoantigen Load Determine Response to PD-L1 Blockade in Extensive-Stage Small Cell Lung Cancer

Short title: Tumor Immune Microenvironment, Neoantigen Load, and ICI Efficacy in SCLC

Hiroaki Kanemura,<sup>a</sup> Hidetoshi Hayashi,<sup>a</sup> Shuta Tomida,<sup>b</sup> Junko Tanizaki,<sup>a,c</sup>  
Shinichiro Suzuki,<sup>a,c</sup> Yusuke Kawanaka,<sup>a,c</sup> Asuka Tsuya,<sup>d</sup> Yasushi Fukuda,<sup>e</sup>  
Hiroyasu Kaneda,<sup>f</sup> Keita Kudo,<sup>g</sup> Takayuki Takahama,<sup>h</sup> Ryosuke Imai,<sup>i</sup> Koji Haratani,<sup>a</sup>  
Yasutaka Chiba,<sup>j</sup> Tomoyuki Otani,<sup>k</sup> Akihiko Ito,<sup>k</sup> Kazuko Sakai,<sup>l</sup> Kazuto Nishio,<sup>l</sup>  
Kazuhiko Nakagawa<sup>a</sup>

<sup>a</sup>Department of Medical Oncology, Kindai University Faculty of Medicine, 377-2 Ohno-higashi, Osaka-Sayama, Osaka 589-8511, Japan

<sup>b</sup>Center for Comprehensive Genomic Medicine, Okayama University Hospital, 2-5-1 Shikata-cho, Kita-ku, Okayama 700-8558, Japan

<sup>c</sup>Department of Medical Oncology, Kishiwada City Hospital, 1001 Gakuhara, Kishiwada, Osaka 596-8501, Japan

<sup>d</sup>Department of Medical Oncology, Izumi City General Hospital, 4-5-1 Wake-cho, Izumi, Osaka 594-0073, Japan

<sup>e</sup>Department of Respiratory Medicine, Kurashiki Central Hospital, 1-1-1 Miwa, Kurashiki, Okayama 710-8602, Japan

<sup>f</sup>Department of Clinical Oncology, Graduate School of Medicine, Osaka City University, 1-5-7 Asahimachi, Abeno-ku, Osaka 545-8602, Japan

<sup>g</sup>Department of Thoracic Medical Oncology, National Hospital Organization Osaka Minami Medical Center, 2-1 Kidohigashi-machi, Kawachinagano, Osaka 586-8521, Japan

<sup>h</sup>Department of Medical Oncology, Kindai University Nara Hospital, 1248-1 Otoda-cho, Ikoma, Nara 630-0293, Japan

<sup>i</sup>Department of Pulmonary Medicine, Thoracic Center, St. Luke's International Hospital, 9-1 Akashi-cho, Chuo-ku, Tokyo 104-8560, Japan

<sup>j</sup>Clinical Research Center, Kindai University Hospital, 377-2 Ohno-higashi, Osaka-Sayama, Osaka 589-8511, Japan

<sup>k</sup>Department of Pathology, Kindai University Faculty of Medicine, 377-2 Ohno-higashi, Osaka-Sayama, Osaka 589-8511, Japan

<sup>l</sup>Department of Genome Biology, Kindai University Faculty of Medicine, 377-2 Ohno-higashi, Osaka-Sayama, Osaka 589-8511, Japan

**\*Corresponding author:** Hidetoshi Hayashi, Department of Medical Oncology, Kindai

University Faculty of Medicine, 377-2 Ohno-higashi, Osaka-Sayama, Osaka 589-8511, Japan. Tel.: +81-72-366-0221. Fax: +81-72-360-5000. Email: hidet31@med.kindai.ac.jp

**Funding/Support:** The biomarker measurement in this study was funded by Chugai Pharmaceutical Co. Ltd.

**Role of the Funder/Sponsor:** Chugai Pharmaceutical Co. Ltd. was involved with review and approval of the conflict of interest disclosure and intellectual property but not with the design and conduct of the study; collection, management, analysis, and interpretation of the data; preparation of the manuscript; and the decision to submit the manuscript for publication.

**Conflict of Interest Disclosures:** Dr. Kanemura has received support for the present study from Chugai Pharmaceutical Co. Ltd. Dr. Hayashi has received support for the present study from Chugai Pharmaceutical Co. Ltd.; honoraria from AstraZeneca K.K., Boehringer Ingelheim Japan Inc., Bristol-Myers Squibb Co. Ltd., Chugai Pharmaceutical Co. Ltd., Eli Lilly Japan K.K., Kyorin Pharmaceutical Co. Ltd., Merck Biopharma Co. Ltd., MSD K.K., Novartis Pharmaceuticals K.K., Ono Pharmaceutical Co. Ltd., Taiho Pharmaceutical Co. Ltd., and Takeda Pharmaceutical Co. Ltd.; consulting fees from AstraZeneca K.K., Boehringer Ingelheim Japan Inc., Bristol-Myers Squibb Co. Ltd., Chugai Pharmaceutical Co. Ltd., Eli Lilly Japan K.K., Pfizer Japan Inc., Shanghai Haihe Biopharma, Takeda Pharmaceutical Co. Ltd., and Merck Biopharma Co. Ltd.; and research funding from AstraZeneca K.K., Astellas Pharma Inc., MSD K.K., Ono Pharmaceutical Co. Ltd., Nippon Boehringer Ingelheim Co. Ltd., Novartis Pharma K.K., Pfizer Japan Inc., Bristol Myers Squibb Co. Ltd., Eli Lilly Japan K.K., Chugai Pharmaceutical Co. Ltd., Daiichi Sankyo Co. Ltd., Merck Serono Co. Ltd./Merck Biopharma Co. Ltd., Takeda Pharmaceutical Co. Ltd., Taiho Pharmaceutical Co. Ltd., Symbio Pharmaceuticals Limited, AbbVie Inc., inVentiv Health Japan, ICON Japan K.K., Gritstone Oncology Inc., Parexel International Corp., Kissei Pharmaceutical Co. Ltd., EPS Corporation, Syneos Health, Pfizer R&D Japan G.K., A2 Healthcare Corp., Quintiles Inc./IQVIA Services Japan K.K., EP-CRSU Co. Ltd., Linical Co. Ltd., Eisai Co. Ltd., CMIC Shift Zero K.K., Kyowa Hakko Kirin Co. Ltd., Bayer Yakuhin Ltd., EPS International Co. Ltd., and Otsuka Pharmaceutical Co. Ltd. Dr. Tomida has received honoraria from Chugai Pharmaceutical Co. Ltd. and Illumina Inc. Dr. Tanizaki has received honoraria from AstraZeneca K.K., Boehringer-Ingelheim Japan Inc., Bristol-Myers Squibb Co. Ltd., Chugai Pharmaceutical Co. Ltd., Eli Lilly Japan K.K., Taiho Pharmaceutical Co. Ltd., and MSD K.K. Dr. Fukuda has received lecture fees from AstraZeneca K.K., Daiichi Sankyo Co. Ltd., Chugai Pharmaceutical Co. Ltd., Merck Biopharma Co. Ltd., MSD K.K., Ono Pharmaceutical Co. Ltd., Taiho Pharmaceutical Co. Ltd., Bristol-Myers Squibb Co. Ltd., Nippon Boehringer Ingelheim Co. Ltd., and Kyorin Pharmaceutical Co. Ltd. Dr. Kaneda has received honoraria from Chugai Pharmaceutical Co. Ltd. and AstraZeneca K.K.

Dr. Takahama has received honoraria from AstraZeneca K.K., Roche Diagnostics, Boehringer Ingelheim Japan Inc., Chugai Pharmaceutical Co. Ltd., and Pfizer Japan Inc.. Dr. Haratani has received honoraria from AS ONE Corp., AstraZeneca K.K., Bristol-Myers Squibb Co. Ltd., Chugai Pharmaceutical Co. Ltd., MSD K.K., and Ono Pharmaceutical Co. Ltd. as well as research funding from AstraZeneca K.K. and MSD K.K. Dr. Chiba has received honoraria from Chugai Pharmaceutical Co. Ltd. Dr. Sakai has received honoraria from Roche Diagnostics, Bio-Rad, AstraZeneca K.K., Chugai Pharmaceutical Co. Ltd., and Hitachi. Dr. Nishio has received honoraria from Boehringer Ingelheim Japan Inc., Chugai Pharmaceutical Co. Ltd., Eisai Co. Ltd., Pfizer Japan Inc., Novartis Pharmaceuticals K.K., MSD K.K., Ono Pharmaceutical Co. Ltd., Bristol-Myers Squibb Co. Ltd., Life Technologies Japan, Yakult Honsha, Roche Diagnostics, AstraZeneca K.K., Sanofi, Guardant Health, Amgen, and Merck Biopharma Co. Ltd.; consulting fees from Solasia Pharma, Otsuka Pharmaceutical Co. Ltd., Eli Lilly Japan K.K., and SymBio Pharmaceuticals; and research funding from Ignyta Inc., Eli Lilly Japan K.K., Nippon Boehringer Ingelheim Co. Ltd., Korea Otsuka Pharmaceutical, and Nichirei Biosciences Inc.. Dr. Nakagawa has received honoraria from AstraZeneca K.K., Chugai Pharmaceutical Co. Ltd., Nippon Kayaku Co. Ltd., Takeda Pharmaceutical Co. Ltd., Ono Pharmaceutical Co. Ltd., Roche Diagnostics K.K., Astellas Pharma Inc., MSD K.K., Bayer Yakuhin Ltd., Eli Lilly Japan K.K., Merck Biopharma Co. Ltd., Kyorin Pharmaceutical Co. Ltd., Thermo Fisher Scientific K.K., Hisamitsu Pharmaceutical Co. Inc., Nanzando Co. Ltd., Daiichi Sankyo Co. Ltd., Novartis Pharma K.K., Kyowa Kirin Co. Ltd., Medical Mobile Communications Co. Ltd., Yomiuri Telecasting Corp., Nikkei Business Publications Inc., Nippon Boehringer Ingelheim Co. Ltd., Medicus Shuppan Publishers Co. Ltd., Taiho Pharmaceutical Co. Ltd., Pfizer Japan Inc., AbbVie Inc., Bristol-Myers Squibb Co. Ltd., CareNet Inc., Amgen Inc., Medical Review Co. Ltd., Yodosha Co. Ltd., 3H Clinical Trial Inc., and Nichi-Iko Pharmaceutical Co. Ltd.; consulting fees from Astellas Pharma Inc., Eli Lilly Japan K.K., Takeda Pharmaceutical Co. Ltd., Pfizer Japan Inc., Ono Pharmaceutical Co. Ltd., and Kyorin Pharmaceutical Co. Ltd.; and research funding from Takeda Pharmaceutical Co. Ltd., Taiho Pharmaceutical Co. Ltd., AbbVie Inc., GlaxoSmithKline K.K., Parexel International Corp., ICON Japan K.K., EPS Corp., Kissei Pharmaceutical Co. Ltd., Pfizer R&D Japan G.K., Syneos Health, IQVIA Services Japan K.K., A2 Healthcare Corp., CMIC Shift Zero K.K., Eisai Co. Ltd., SymBio Pharmaceuticals Limited., Kyowa Kirin Co. Ltd., Bayer Yakuhin Ltd., EPS International Co. Ltd., Otsuka Pharmaceutical Co. Ltd., PRA Health Sciences, Covance Japan Inc., Medical Research Support, Sanofi K.K., PPD-SNBL K.K., Japan Clinical Research Operations, Sysmex Corp., and Mochida Pharmaceutical Co. Ltd. All remaining authors have declared no conflicts of interest.

## **ABSTRACT**

**Introduction:** Despite a significant benefit of adding immune checkpoint inhibitors (ICIs) to platinum-based chemotherapy for patients with extensive-stage small cell lung cancer (ES-SCLC), a durable response to ICIs occurs in only a small minority of such patients.

**Methods:** A total of 135 patients with ES-SCLC treated with chemotherapy either alone (chemo-cohort, n=71) or together with an ICI (ICI combo-cohort, n=64) was included in this retrospective study. Tumors were classified pathologically as inflamed or noninflamed on the basis of programmed cell death–ligand 1 (PD-L1) expression and CD8<sup>+</sup> tumor-infiltrating lymphocyte density. Immune-related gene expression profiling (irGEP) was performed, and predicted neoantigen load was determined by whole-exome sequencing.

**Results:** Among patients in the ICI combo-cohort, median progression-free survival (PFS) was 10.8 and 5.1 months for those with inflamed (n=7) or noninflamed (n=56) tumors, respectively (log-rank test  $P=0.002$ ; hazard ratio of 0.26). Among the 89 patients with irGEP data available, inflamed tumors had a higher T cell–inflamed GEP score than did noninflamed tumors ( $-0.18$  versus  $-0.58$ ,  $P<0.001$ ). The 12-month PFS rate was 16.1% and 0% for patients in the ICI combo-cohort harboring tumors with a high (n=26) or low (n=18) frameshift neoantigen load, respectively. A high frameshift neoantigen load was associated with up-regulation of gene signatures related to antigen presentation and costimulatory signaling. A durable clinical benefit of ICI therapy was observed only in patients with inflamed tumors and a high frameshift neoantigen load.

**Conclusions:** Expression of PD-L1, CD8<sup>+</sup> T cell infiltration, and a high frameshift neoantigen load are associated with clinical benefit of ICI therapy in ES-SCLC.

**Clinical trial registration:** UMIN000041056

**Keywords:** Small cell lung cancer; Immunotherapy; Tumor-infiltrating lymphocyte; Tumor mutation burden; Neoantigen

### **Abbreviations**

CI, confidence interval; CPS, combined positive score; ES-SCLC, extensive-stage small cell lung cancer; FDR, false discovery rate; fs-indel, frameshift insertion-deletion; HLA, human leukocyte antigen; HR, hazard ratio; ICI, immune checkpoint inhibitor; IHC, immunohistochemistry; irGEP, immune-related gene expression profiling; LUAD, lung adenocarcinoma; MHC, major histocompatibility complex; nsSNV, nonsynonymous single nucleotide variant; PD-L1, programmed cell death–ligand 1; PFS, progression-free survival; TCGA, The Cancer Genome Atlas; TIL, tumor-infiltrating lymphocyte; TMB, tumor mutation burden; TME, tumor immune microenvironment; TPS, tumor proportion score; WES, whole-exome sequencing.

## **Introduction**

Small cell lung cancer (SCLC) is an aggressive high-grade neuroendocrine tumor with a low survival rate. It accounts for ~15% of lung cancer cases worldwide and is the sixth leading cause of cancer-related death.<sup>1-3</sup> The standard treatment for SCLC remained unchanged for several decades, with no improvement in survival time.<sup>4</sup> Recently, however, phase 3 trials have demonstrated a significant survival advantage for the addition of antibodies to programmed cell death–ligand 1 (PD-L1) to first-line chemotherapy for extensive-stage SCLC (ES-SCLC),<sup>5,6</sup> although the benefit of this new treatment strategy is restricted to a small subset of patients, in part because of a limited understanding of both the disease and the key determinants of a response to immunotherapy.<sup>7,8</sup>

SCLC is strongly associated with smoking and therefore has a relatively high tumor mutation burden (TMB), suggesting that it might be responsive to immune checkpoint inhibitors (ICIs).<sup>9-12</sup> However, only ~20% of SCLC tumors have a tumor proportion score (TPS) for PD-L1 of  $\geq 1\%$ .<sup>13-16</sup> A better understanding of the transcriptomic and genomic features of SCLC is therefore needed to inform the development of optimal therapeutic strategies.

We hypothesized that a comprehensive molecular analysis of the tumor immune microenvironment (TME) and genomic underpinnings of tumor antigenicity for SCLC might reveal immunologic determinants of the response or resistance to immunotherapy and thereby support both the identification of patients likely to derive the most benefit from such treatment and the development of new therapeutic approaches. We have therefore now performed an exploratory study to characterize the pathological, transcriptomic, and genetic immune profiles of SCLC.

## **Methods**

### ***Patients***

We reviewed the medical records of all individuals with pathologically confirmed ES-SCLC treated at the study hospitals between January 2015 and January 2021. Patients diagnosed on the basis of cytology only or with insufficient residual tissue specimens were excluded from biomarker analysis. The chemo-cohort comprised patients treated with platinum-based chemotherapy without an ICI, whereas the ICI combo-cohort comprised those treated with such chemotherapy in combination with an ICI. Among individuals who received prior chemoradiotherapy for limited-stage SCLC, those who had been treated with curative intent and experienced a treatment-free interval of at least 6 months after the last chemotherapy, radiotherapy, or chemoradiotherapy cycle and before the diagnosis of ES-SCLC were also included. The study was conducted according to the Declaration of Helsinki and protocols approved by the Institutional Review Board (IRB) of each participating hospital. All patients provided written informed consent, where applicable, or such informed consent was waived by IRB-approved protocols for aggregate deidentified data analysis.

### ***Data Collection***

Medical records were reviewed, and data regarding clinicopathologic features and treatment history were extracted. The data cutoff date was 30 June 2021. Tumor response was assessed by computed tomography every 6 to 8 weeks according to Response Evaluation Criteria in Solid Tumors, version 1.1.<sup>17</sup> Progression-free survival (PFS) was measured from treatment initiation to clinical or radiographic progression or death from any cause. Patients without documented clinical or radiographic disease progression were censored on the date of last follow-up.

### ***Statistical Analysis***

Categorical and continuous variables were summarized descriptively as percentage and median values. Differences in continuous variables were assessed with the Wilcoxon rank sum test, and those in categorical variables with Fisher's exact test. Comparisons among more than two groups were performed with Dunn's test. Correlations were examined with the Spearman correlation test. The Benjamini-Hochberg method was applied to calculate the false discovery rate (FDR) for multiple testing. Differences in PFS curves constructed by the Kaplan-Meier method were assessed with the log-rank test, and the Cox proportional hazard regression model was adopted to determine hazard ratios (HRs). All *P* values are two-sided and confidence intervals (CIs) are at the 95% level, with statistical significance defined as a *P* value of <0.05 (with the exception of Dunn's test, *P* < 0.025). Statistical analysis was performed with Stata/IC version 14.2 (StataCorp LP) or GraphPad Prism 7.0 (GraphPad Software).

### ***Assessment of Pathological, Transcriptomic, and Genetic Immune Profiles***

Protocols for immunohistochemistry (IHC), assessment of immune-related gene expression, and whole-exome sequencing (WES) are described in Supplementary Methods.

## **Results**

### ***Patient Characteristics***

A total of 135 patients who were treated between January 2015 and January 2021 and who had baseline tissue specimens available was enrolled, 71 patients in the chemo-cohort and 64 patients in the ICI combo-cohort. Patient flow is summarized in **Supplementary Figure S1**. Demographic characteristics were well balanced between the two cohorts (**Table 1**).

### ***TME Classification on the Basis of PD-L1 Expression and CD8<sup>+</sup> TIL Density***

Median follow-up time was 32.9 months (range, 0.6–37.8 months) for the chemo-cohort and 15.9 months (range, 1.8–20.8 months) for the ICI combo-cohort. Median PFS was 4.8 months (95% CI, 4.2–5.3 months) and 5.3 months (95% CI, 4.6–5.7 months) in the chemo-cohort and

ICI combo-cohort, respectively. The 12-month PFS rate was 4.4% (95% CI, 1.1–11.1%) and 11.1% (95% CI, 4.9–20.2%) in the chemo-cohort and ICI combo-cohort, respectively (**Supplementary Fig. S2**).

The 133 patients for whom both PD-L1 and CD8 expression data were available were stratified into four TME groups on the basis of cutoffs of 1% for PD-L1 combined positive score (CPS) and of the median (85/mm<sup>2</sup>) for CD8<sup>+</sup> tumor-infiltrating lymphocyte (TIL) density (**Fig. 1A**). We defined PD-L1<sup>positive</sup> (CPS of  $\geq 1\%$ ) and CD8<sup>+</sup> TIL<sup>high</sup> ( $>85/\text{mm}^2$ ) tumors on the basis of this stratification as “inflamed tumors,” and all other tumors as “noninflamed tumors.” For the ICI combo-cohort (n = 63), median PFS was 10.8 months (95% CI, 3.5 months–not reached; n = 7) in patients with inflamed tumors versus 5.1 months (95% CI, 4.3–5.6 months; n = 56) in those with noninflamed tumors (log-rank test  $P = 0.002$ ; HR of 0.26, with a 95% CI of 0.09–0.74), with 12-month PFS rates of 42.9% (95% CI, 9.8–73.4%) and 5.5% (95% CI, 1.4–13.7%), respectively (**Fig. 1B**). In contrast, for the chemo-cohort (n = 70), there was no significant difference in PFS between inflamed and noninflamed tumors (median of 3.6 months [95% CI, 3.1–5.5 months] versus 4.8 months [95% CI, 4.4–5.7 months], respectively; log-rank test  $P = 0.11$ ; HR of 1.70, with a 95% CI of 0.92–3.14), with 12-month PFS rates of 0% and 5.5% (95% CI, 1.5–13.8%), respectively (**Fig. 1C**). These results suggested that the combination of PD-L1 CPS and CD8<sup>+</sup> TIL density might serve as a potential biomarker for patient selection with regard to immunotherapy in SCLC.

### ***Transcriptomic Features of the TME According to PD-L1 Expression and CD8<sup>+</sup> TIL Density***

We next performed immune-related gene expression profiling (irGEP) for 50 and 39 tumor samples obtained from the chemo-cohort and ICI combo-cohort, respectively, in order to evaluate the immune profile of SCLC in more detail. A T cell–inflamed GEP score was calculated as a weighted sum of normalized expression values for 18 genes, as described previously,<sup>18</sup> with this score having been found to be associated with benefit of immunotherapy in solid tumors.<sup>19</sup> Among the 89 studied patients, the 17 individuals with inflamed tumors had a higher T cell–inflamed GEP score than did the 72 individuals with noninflamed tumors (–0.18 versus –0.58,  $P < 0.001$ ) (**Fig. 2A**).

We further investigated the immunologic characteristics of inflamed tumors (n = 17) and noninflamed tumors (n = 72). We thus performed unsupervised analysis of 676 immune-related genes for the 89 samples subjected to irGEP (**Fig. 2B**). On the basis of the hierarchical clustering for the 89 patients shown in **Figure 2B**, we selected two gene clusters that were expressed at a higher level in inflamed tumors (cluster 1, 217 genes) or in noninflamed tumors (cluster 2, 169 genes). Cluster 1 (n = 217 genes) contained genes related to costimulatory T cell signaling (n = 26 genes, including *CD48*, *CD80*, *CD274*, *IL18*, *LILRB2*, *PTPRC*, *IL2RA*, and *IL15*), to cytokine and chemokine signaling (n = 25 genes, including

*CXCL10*, *IL2RA*, *IL10RA*, and *JAK3*), and to antigen presentation (n = 34 genes, including *CTSS* and *HLA-DRA*, *-DMA*, *-DMB*, *-DOA*, *-DPA1*, and *-DPB1*). In contrast, cluster 2 (n = 169 genes) contained genes related to cell proliferation (n = 28 genes, including *ANLN*, *BIRC5*, *CCNE1*, *CENPF*, *MKI67*, *MELK*, *RRM2*, *TYMS*, *TP53*, and *UBE2C*) and to DNA damage repair (n = 20 genes, including *BRCA1*, *BRCA2*, *BRIP1*, *EXO1*, *MSH2*, *MSH6*, and *UBE2T*).

We also examined differential expression of individual genes with the 89 tumor specimens to shed light on differentially enriched processes in inflamed tumors versus noninflamed tumors. Genes related to cytotoxic lymphocytes (such as *GZMA*), to costimulatory molecules (such as *CD274* and *TIGIT*), and to cytokine and chemokine signaling (such as *IL2RG*, *IL2RA*, *CXCL9*, and *CXCL10*) were among those expressed at a significantly higher level in inflamed tumors (**Fig. 2C**, **Supplementary Fig. S3A**). In contrast, *SOX11* ( $P < 0.001$ , FDR  $< 0.001$ ) and *MYC* ( $P = 0.02$ , FDR = 0.06) were the top two up-regulated genes in noninflamed tumors relative to inflamed tumors, suggesting that *SOX11* and *MYC* might contribute to poor immunoreactivity in SCLC (**Fig. 2C**, **Supplementary Fig. S3A**). We further investigated whether *MYC* might be a determinant of ICI efficacy. Patients in each cohort were divided into two groups according to the median value for *MYC* expression (**Supplementary Fig. S4**). For the ICI combo-cohort (n = 39), median PFS was 4.0 months (95% CI, 3.1–5.4 months; n = 22) in patients with *MYC*<sup>high</sup> tumors versus 5.3 months (95% CI, 4.6–7.3 months; n = 17) in those with *MYC*<sup>low</sup> tumors (log-rank test  $P = 0.028$ ; HR of 2.18, with a 95% CI of 1.08–4.40), with 12-month PFS rates of 4.6% (95% CI, 0.3–18.9%) and 23.5% (95% CI, 7.3–44.9%), respectively. In contrast, for the chemo-cohort (n = 50), there was no significant difference in PFS between *MYC*<sup>high</sup> and *MYC*<sup>low</sup> tumors (median of 4.8 months [95% CI, 3.6–5.5 months; n = 23] versus 4.9 months [95% CI, 4.3–5.9 months; n = 27], respectively; log-rank test  $P = 0.77$ ; HR of 1.09, with a 95% CI of 0.61–1.94). These results thus indicated that *MYC* expression was negatively associated with ICI efficacy.

Among the up-regulated genes in inflamed tumors, *TIGIT* encodes a member of the immunoglobulin superfamily of proteins that is expressed on the surface of T cells and natural killer cells and which has recently been examined as a potentially targetable immune checkpoint molecule.<sup>20</sup> We found that the expression level of *TIGIT* was moderately correlated with TIGIT<sup>+</sup> TIL density as determined by IHC (Spearman correlation coefficient [ $r$ ] = 0.32,  $P = 0.006$ ) (**Supplementary Fig. S3B**), and that TIGIT<sup>+</sup> TIL density was significantly higher in inflamed tumors than in noninflamed tumors (75/mm<sup>2</sup> [95% CI, 25–144/mm<sup>2</sup>] versus 25/mm<sup>2</sup> [95% CI, 25–25/mm<sup>2</sup>],  $P = 0.002$ ) (**Fig. 2D**, **Supplementary Fig. S3C**). These findings thus implicated TIGIT as a potentially targetable molecule in inflamed tumors.

Moreover, our data showed that the expression of gene signatures related to cell proliferation or to DNA damage repair was significantly higher in noninflamed tumors than

in inflamed tumors (**Fig. 2E**). The expression of these gene signatures was inversely correlated with that of other immune-related pathway signatures in the 89 tumor specimens analyzed (**Supplementary Fig. S3D**).

Collectively, our irGEP analysis suggested that a T cell–inflamed gene expression profile might play an important role in promoting anticancer immunity, with the increased expression of genes related to costimulatory signaling, cytokine and chemokine signaling, and antigen presentation providing a potential explanation for the more favorable response of inflamed tumors to ICIs. Conversely, up-regulation of gene signatures related to cell proliferation and DNA damage repair might contribute to the acquisition of an immunosuppressive phenotype. The mechanisms by which cell proliferation and DNA damage repair might contribute to ICI efficacy require further investigation.

### ***Genomic Features of Tumor Antigenicity in SCLC***

TMB is an indirect measure of tumor antigenicity and might play a role in the recognition of cancer cells by the immune system.<sup>21, 22</sup> Tumor neoantigens are mutant peptides generated as a result of genetic mutations and are capable of eliciting an antitumor T cell response.<sup>23, 24</sup> Although SCLC has a high TMB and would therefore be expected to induce a strong T cell response, the response to ICIs is limited to <15% of SCLC patients.<sup>25, 26</sup> Neoantigens generated by insertion-deletion (indel) mutations have been found to be enriched relative to those generated by nonsynonymous single nucleotide variants (nsSNVs) in various cancer types.<sup>21</sup> Furthermore, a high load of frameshift neoantigens was associated with increased expression of genes related to immune activation, whereas a high load of nsSNV neoantigens was not.<sup>21</sup> On the basis of these findings, we defined TMB broadly in our study as the total number of SNVs (synonymous and nonsynonymous) and indels per tumor genomic region analyzed. In addition, our bioinformatics pipelines for the prediction of neoantigens focused on those derived from nsSNVs and frameshift indels (fs-indels).

We first compared the distribution of TMB between SCLC and lung adenocarcinoma (LUAD), with WES data for 20 LUAD patients (top 10 and bottom 10 TMB samples) being obtained from The Cancer Genome Atlas (TCGA). As expected, the SCLC tumors in our cohort ( $n = 85$ ) had a higher TMB compared with LUAD tumors with the top 10 highest TMB values from TCGA (median TMB of 6.8/Mb [95% CI, 6.0–7.6/Mb] versus 2.9/Mb [95% CI, 2.1–5.3/Mb],  $P < 0.001$ ) (**Fig. 3A**).

We next examined the relation of TMB to PFS in the ICI combo-cohort of our SCLC patients ( $n = 44$ ). PFS did not differ significantly between patients with a high versus low TMB (median of 5.1 months [95% CI, 3.9–6.5 months] versus 5.6 months [95% CI, 4.3–6.3 months], respectively; log-rank test  $P = 0.93$ ; HR of 0.97, with a 95% CI of 0.52–1.83), with 12-month PFS rates of 12.5% (95% CI, 3.1–28.7%) and 5.3% (95% CI, 0–21.5%), respectively (**Fig. 3B**). Similarly, in the chemo-cohort ( $n = 41$ ), the median PFS was 5.3 months (95% CI, 3.8–6.4 months) for the high-TMB group and 4.4 months (95% CI, 3.2–5.1

months) for the low-TMB group (log-rank test  $P = 0.18$ ; HR of 0.64, with a 95% CI of 0.34–1.23), with corresponding 12-month PFS rates of 11.8% (95% CI, 0.4–21.9%) and 0% (**Supplementary Fig. S5A**). These findings suggested that a high TMB was not associated with a clinical benefit of ICI treatment.

We next investigated the potential immunogenicity of nsSNVs and fs-indels in SCLC by prediction of major histocompatibility complex (MHC) class I-associated neoantigens (**Table 2**). Analysis of the total of 21,059 nsSNVs detected in the 85 SCLC tumors predicted 3299 high-affinity neoantigens (defined as epitopes with a predicted binding affinity of  $<50$  nM), corresponding to a rate of 0.16 neoantigens per nsSNV. Similar analysis for the total of 1346 fs-indels predicted 662 high-affinity binders, corresponding to a rate of 0.49 neoantigens per fs-indel. Frameshift mutations were thus predicted to generate three times as many neoantigens per mutation as were SNVs, consistent with recent findings for various cancer types.<sup>21</sup> We performed the same analysis for the TCGA-LUAD data set and found that fs-indels were predicted to give rise to five or 30 times as many neoantigens as were nsSNVs for the top 10 and bottom 10 tumors ranked according to TMB, respectively (**Table 2**). We then defined the proportion of fs-indels for each tumor as the number of fs-indels divided by the total number of indels and SNVs. The median number of fs-indels tended to be lower in SCLC than in the top 10 LUAD tumors ranked by TMB (13 [95% CI, 10–15] versus 20 [95% CI, 13–34],  $P = 0.03$ ) (**Fig. 3C**), and the proportion of fs-indels in SCLC was significantly lower than in these 10 LUAD tumors (0.018 [95% CI, 0.015–0.021] versus 0.86 [95% CI, 0.41–1.37],  $P < 0.001$ ) (**Fig. 3D**). These findings suggested that the lower number and proportion of fs-indels, and consequent lower load of frameshift neoantigens, might contribute to the limited efficacy of ICIs in SCLC compared with LUAD.

We next calculated PFS according to predicted frameshift neoantigen load in the ICI combo-cohort of our SCLC patients ( $n = 44$ ). The patients were thus split into two groups on the basis of the median number of frameshift neoantigens. The median PFS was 5.7 months (95% CI, 4.1–6.8 months) for the high-frameshift neoantigen group and 5.1 months (95% CI, 4.3–5.6 months) for the low-frameshift neoantigen group (log-rank test  $P = 0.12$ ; HR of 0.60, with a 95% CI of 0.31–1.14), with corresponding 12-month PFS rates of 16.1% (95% CI, 5.1–32.7%) and 0%, respectively (**Fig. 3E**). PFS thus tended to be more favorable for the high-frameshift neoantigen group. In the chemo-cohort ( $n = 41$ ), median PFS was 5.1 months (95% CI, 4.2–6.0 months) for the high-frameshift neoantigen group and 4.6 months (95% CI, 3.1–5.6 months) for the low-frameshift neoantigen group (log-rank test  $P = 0.92$ ; HR of 0.97, with a 95% CI of 0.51–1.83), with 12-month PFS rates of 5.4% (95% CI, 0.4–21.9%) and 5.0% (95% CI, 0.4–20.5%), respectively (**Supplementary Fig. S5B**). Our analysis thus suggested that the number of frameshift neoantigens was more associated with clinical benefit from ICIs than was TMB.

### *Association of Immune Signatures Related to Antigen Presentation or Costimulatory*

### ***Signaling with Frameshift Neoantigens***

To explore further the different effects of TMB and frameshift neoantigen load on immune responses, we examined the relation between these two parameters and immune-related gene expression. SCLC patients were split into groups on the basis of the median values of TMB (high defined as  $\geq 6.85/\text{Mb}$ ) and frameshift neoantigen load (high defined as  $\geq 5$  frameshift neoantigens per case). A high load of frameshift neoantigens was associated with a high expression level for immune signatures related to antigen presentation and to costimulatory signaling, whereas a high TMB was associated with a high expression level for immune signatures related to cell proliferation and to DNA damage repair (**Fig. 4A**). These findings were similar to the differences in gene expression signatures between inflamed and noninflamed tumors (**Fig. 2B–E**), consistent with the notion that frameshift neoantigen load is associated with ICI efficacy in SCLC.

We next examined the relation between frameshift neoantigen load and the T cell–inflamed GEP score, which we found was higher in inflamed tumors than in noninflamed tumors (**Fig. 2A**). There was no correlation between these measures (**Fig. 4B**), suggesting that the effect of frameshift neoantigen load on ICI efficacy was independent of the T cell–inflamed GEP score.

Finally, we evaluated the clinical utility of the combination of inflammation category (inflamed or noninflamed) and frameshift neoantigen load. Among the 64 patients in the ICI combo-cohort, the 24 individuals with available data were stratified into four groups on the basis of inflammation category and the median frameshift neoantigen load (high defined as  $\geq 5$  frameshift neoantigens per case). A durable clinical benefit (PFS of  $\geq 12$  months) was apparent only in patients with both inflamed tumors and a high frameshift neoantigen load (**Fig. 4C**). Collectively, these results suggested that the expression of PD-L1 and CD8<sup>+</sup> T cell infiltration, together with a high frameshift neoantigen load associated with the up-regulation of gene expression signatures related to antigen presentation and costimulatory signaling, might confer a durable clinical benefit of ICI therapy in SCLC.

### **Discussion**

Our results have revealed that PD-L1 expression and CD8<sup>+</sup> TIL density together are able to predict which ES-SCLC patients are likely to derive clinical benefit from the combination of platinum-based chemotherapy and ICI therapy. In addition, a high frameshift neoantigen load tended to be more associated with clinical benefit from ICI treatment than was a high TMB. Our irGEP analysis implicated a T cell–inflamed TME primed for a response to immunotherapy as well as up-regulation of gene expression related to costimulatory signaling, cytokine and chemokine signaling, and antigen presentation as determinants of the antitumor immune response.

Although classification of tumors into groups on the basis of PD-L1 status and the presence of TILs has been proposed for other cancer types,<sup>27,28</sup> SCLC has not previously

been evaluated for the relation between immune characteristics and clinical outcome of chemo-immunotherapy. Not unexpectedly, we found that pathologically inflamed SCLC tumors as defined on the basis of PD-L1 expression level and CD8<sup>+</sup> TIL density received a greater benefit from anticancer immunotherapy. We also identified additional distinct transcriptomic features of these tumors including the up-regulation of gene expression related to costimulatory signaling, cytokine and chemokine signaling, and antigen presentation.

Consistent with the finding that 12.6% of ES-SCLC patients received a durable clinical benefit (PFS of  $\geq 12$  months) from chemotherapy plus an ICI in the IMpower133 trial,<sup>5</sup> 11.1% of the ES-SCLC patients in our cohort showed such a benefit. In our cohort, 85% of patients were classified as having noninflamed tumors. Although a phase 3 trial showed no benefit from adding an antibody to cytotoxic T lymphocyte antigen-4 (CTLA-4) as well as an anti-PD-L1 antibody to platinum-based chemotherapy for ES-SCLC patients,<sup>8</sup> our results suggest that the ~85% of patients with noninflamed tumors might be amenable to combination therapy designed to promote T cell infiltration. On the other hand, 15% of our ES-SCLC patients were classified as having inflamed tumors, but, among the seven of these patients in the ICI combo-cohort, only three showed a durable clinical benefit (PFS of  $\geq 12$  months). Moreover, given that TIGIT<sup>+</sup> TIL density was significantly higher in inflamed tumors than in noninflamed tumors, the combination of an agent that targets TIGIT with a currently available ICI might be a promising treatment approach. A large phase 3 trial (NCT04256421, SKYSCRAPER-02) of the TIGIT inhibitor tiragolumab in combination with atezolizumab-carboplatin-etoposide for ES-SCLC is currently ongoing.<sup>29</sup>

Our exploratory irGEP analysis provided insight into the mechanisms underlying the limited efficacy of ICIs for SCLC, with gene expression signatures related to DNA damage repair and cell proliferation as well as the expression of *SOX11* and *MYC* being implicated in the lack of immunogenicity. Previous studies have found that genes related to DNA damage repair are expressed at a higher level in SCLC than in LUAD, and that SCLC becomes dependent on such repair pathways for tumor maintenance.<sup>30-32</sup> *SOX11* is a neuronal differentiation factor and promotes neuroendocrine differentiation of cancer.<sup>33, 34</sup> Neuroendocrine-high SCLC was recently found to be associated with reduced levels of immune cell infiltration and expression of immune checkpoint-related molecules including PVR, IDO, MHC class II, and TIM3 compared with neuroendocrine-low SCLC.<sup>35, 36</sup> *SOX11* might therefore contribute to immunosuppression by inducing neuroendocrine differentiation in SCLC. The *MYC* proto-oncogene encodes a transcription factor that is overexpressed in many human cancer types, and dysregulation of *MYC* signaling is implicated in the molecular and histological heterogeneity of SCLC.<sup>37, 38</sup> Although *MYC* activation may influence the antitumor immune response through regulation of CD47 and PD-L1,<sup>37</sup> its role in the responsiveness of SCLC to ICI therapy remains under investigation.<sup>39</sup>

TMB has emerged as a potential biomarker for the efficacy of programmed cell death-1 (PD-1) inhibitors in several tumor types.<sup>10</sup> However, TMB was not predictive of

improvement in overall survival by chemo-immunotherapy in ES-SCLC,<sup>40</sup> and we found that a high TMB was not associated with clinical benefit from ICI treatment in our cohort. Instead, we found that PFS in the ICI combo-cohort tended to be more favorable for patients whose tumors had a high frameshift neoantigen load, although the number of patients in this analysis was relatively small. We also found that a high frameshift neoantigen load was associated with up-regulation of gene expression related to antigen presentation and costimulatory signaling, whereas a high TMB was associated with that of gene expression related to cell proliferation and DNA damage repair. As far as we are aware, our study is the first to have analyzed neoantigen load in SCLC and to suggest the importance of frameshift neoantigens instead of TMB as a determinant of ICI efficacy. The benefit of ICIs for SCLC is limited compared with that apparent for other solid tumor types, despite the high TMB of SCLC attributable to its association with tobacco exposure.<sup>1</sup> Our neoantigen prediction analysis now suggests that the low number and proportion of fs-indels in SCLC compared with LUAD might account for the limited efficacy of ICIs.

Although a strength of our study is the inclusion of two different treatment cohorts, the chemo-cohort and the ICI combo-cohort, our study also has several limitations. First, the study was retrospective in nature and the number of patients was relatively small, precluding multivariate analysis and analysis of a validation cohort. However, with the exception of histology in the ICI combo-cohort and central nervous system metastasis in the chemo-cohort, patient characteristics—including performance status, age, and circulating albumin and lactate dehydrogenase levels—were well balanced between individuals with inflamed or noninflamed tumors in the ICI-combo cohort (**Supplementary Table S1**) and the chemo-cohort (**Supplementary Table S2**). Second, our molecular data were derived from conventional bulk analysis, involving the processing of a mixture of cell types, and the study was thus not able to assess tumor heterogeneity. Third, we could not evaluate the relation between clinical outcome and the four SCLC subtypes defined by differential expression of the transcription factors ASCL1, NEUROD1, and POU2F3 or low expression of all three transcription factors (SCLC-A, -N, -P, and -I, respectively).<sup>41, 42</sup> Retrospective analysis of the IMpower133 trial found that the SCLC-inflamed (SCLC-I) subtype responded best to ICI therapy.<sup>42</sup> SCLC-I tumors manifest high PD-L1 expression and inflammatory features including high expression of human leukocyte antigen (HLA) genes and genes related to interferon activation and immune checkpoints,<sup>42</sup> and they are therefore similar to the inflamed tumors in our study. We found that 15% of SCLC patients had inflamed tumors, similar to the frequency of 18% for SCLC-I tumors in IMpower133.

In conclusion, the classification of ES-SCLC tumors into inflamed and noninflamed subtypes on the basis of PD-L1 expression and CD8<sup>+</sup> TIL density is a simple approach supported by gene expression analysis to the identification of patients likely to benefit most from the addition of an ICI to chemotherapy. In addition to expression of PD-L1 and CD8<sup>+</sup> T cell infiltration, a high frameshift neoantigen load was associated with a durable clinical

benefit from ICI therapy in ES-SCLC. Our study thus provides insight into the pathological, transcriptomic, and genetic immune profiles of SCLC. Further investigation of inflamed and noninflamed tumors should inform personalized treatment strategies and identify treatment resistance mechanisms in SCLC.

**Acknowledgements:** We thank all the patients and medical staff at the participating institutions who contributed to this study; Atsushi Doi (Cell Innovator Inc., Fukuoka, Japan) for technical assistance with WES analysis; as well as Mami Kitano, Haruka Sakamoto, Michiko Kitano, and Yume Shinkai (Department of Medical Oncology, Kindai University Faculty of Medicine) for technical support.

## References

1. Rudin CM, Brambilla E, Faivre-Finn C, et al. Small-cell lung cancer. *Nat Rev Dis Primers* 2021;7:3.
2. Gazdar AF, Bunn PA, Minna JD. Small-cell lung cancer: what we know, what we need to know and the path forward. *Nat Rev Cancer* 2017;17:725-737.
3. Sabari JK, Lok BH, Laird JH, et al. Unravelling the biology of SCLC: implications for therapy. *Nat Rev Clin Oncol* 2017;14:549-561.
4. Howlader N, Forjaz G, Mooradian MJ, et al. The Effect of Advances in Lung-Cancer Treatment on Population Mortality. *N Engl J Med* 2020;383:640-649.
5. Horn L, Mansfield AS, Szczesna A, et al. First-Line Atezolizumab plus Chemotherapy in Extensive-Stage Small-Cell Lung Cancer. *N Engl J Med* 2018;379:2220-2229.
6. Paz-Ares L, Dvorkin M, Chen Y, et al. Durvalumab plus platinum–etoposide versus platinum–etoposide in first-line treatment of extensive-stage small-cell lung cancer (CASPIAN): a randomised, controlled, open-label, phase 3 trial. *The Lancet* 2019;394:1929-1939.
7. Liu SV, Reck M, Mansfield AS, et al. Updated Overall Survival and PD-L1 Subgroup Analysis of Patients With Extensive-Stage Small-Cell Lung Cancer Treated With Atezolizumab, Carboplatin, and Etoposide (IMpower133). *Journal of Clinical Oncology* 2021;39:619-630.
8. Goldman JW, Dvorkin M, Chen Y, et al. Durvalumab, with or without tremelimumab, plus platinum–etoposide versus platinum–etoposide alone in first-line treatment of extensive-stage small-cell lung cancer (CASPIAN): updated results from a randomised, controlled, open-label, phase 3 trial. *The Lancet Oncology* 2021;22:51-65.
9. Alexandrov LB, Nik-Zainal S, Wedge DC, et al. Signatures of mutational processes in human cancer. *Nature* 2013;500:415-421.
10. Yarchoan M, Hopkins A, Jaffee EM. Tumor Mutational Burden and Response Rate to PD-1 Inhibition. *N Engl J Med* 2017;377:2500-2501.
11. Rekhtman N, Pietanza MC, Hellmann MD, et al. Next-Generation Sequencing of Pulmonary Large Cell Neuroendocrine Carcinoma Reveals Small Cell Carcinoma-like and Non-Small Cell Carcinoma-like Subsets. *Clin Cancer Res* 2016;22:3618-3629.
12. Chalmers ZR, Connelly CF, Fabrizio D, et al. Analysis of 100,000 human cancer genomes reveals the landscape of tumor mutational burden. *Genome Med* 2017;9:34.
13. Carvajal-Hausdorf D, Altan M, Velcheti V, et al. Expression and clinical significance of PD-L1, B7-H3, B7-H4 and TILs in human small cell lung Cancer (SCLC). *J Immunother Cancer* 2019;7:65.
14. Bonanno L, Pavan A, Dieci MV, et al. The role of immune microenvironment in small-cell lung cancer: Distribution of PD-L1 expression and prognostic role of FOXP3-positive tumour infiltrating lymphocytes. *Eur J Cancer* 2018;101:191-200.
15. Yu H, Batenchuk C, Badzio A, et al. PD-L1 Expression by Two Complementary

Diagnostic Assays and mRNA In Situ Hybridization in Small Cell Lung Cancer. *J Thorac Oncol* 2017;12:110-120.

16. Schultheis AM, Scheel AH, Ozretic L, et al. PD-L1 expression in small cell neuroendocrine carcinomas. *Eur J Cancer* 2015;51:421-426.
17. Eisenhauer EA, Therasse P, Bogaerts J, et al. New response evaluation criteria in solid tumours: revised RECIST guideline (version 1.1). *Eur J Cancer* 2009;45:228-247.
18. Ayers M, Lunceford J, Nebozhyn M, et al. IFN-gamma-related mRNA profile predicts clinical response to PD-1 blockade. *J Clin Invest* 2017;127:2930-2940.
19. Ott PA, Bang YJ, Piha-Paul SA, et al. T-Cell-Inflamed Gene-Expression Profile, Programmed Death Ligand 1 Expression, and Tumor Mutational Burden Predict Efficacy in Patients Treated With Pembrolizumab Across 20 Cancers: KEYNOTE-028. *J Clin Oncol* 2019;37:318-327.
20. Zhang Q, Bi J, Zheng X, et al. Blockade of the checkpoint receptor TIGIT prevents NK cell exhaustion and elicits potent anti-tumor immunity. *Nat Immunol* 2018;19:723-732.
21. Turajlic S, Litchfield K, Xu H, et al. Insertion-and-deletion-derived tumour-specific neoantigens and the immunogenic phenotype: a pan-cancer analysis. *The Lancet Oncology* 2017;18:1009-1021.
22. Cristescu R, Mogg R, Ayers M, et al. Pan-tumor genomic biomarkers for PD-1 checkpoint blockade-based immunotherapy. *Science* 2018;362.
23. Smith CC, Selitsky SR, Chai S, et al. Alternative tumour-specific antigens. *Nat Rev Cancer* 2019;19:465-478.
24. De Mattos-Arruda L, Vazquez M, Finotello F, et al. Neoantigen prediction and computational perspectives towards clinical benefit: recommendations from the ESMO Precision Medicine Working Group. *Ann Oncol* 2020;31:978-990.
25. Ready NE, Ott PA, Hellmann MD, et al. Nivolumab Monotherapy and Nivolumab Plus Ipilimumab in Recurrent Small Cell Lung Cancer: Results From the CheckMate 032 Randomized Cohort. *J Thorac Oncol* 2020;15:426-435.
26. Chung HC, Piha-Paul SA, Lopez-Martin J, et al. Pembrolizumab After Two or More Lines of Previous Therapy in Patients With Recurrent or Metastatic SCLC: Results From the KEYNOTE-028 and KEYNOTE-158 Studies. *J Thorac Oncol* 2020;15:618-627.
27. Teng MW, Ngiow SF, Ribas A, et al. Classifying Cancers Based on T-cell Infiltration and PD-L1. *Cancer Res* 2015;75:2139-2145.
28. Taube JM, Anders RA, Young GD, et al. Colocalization of Inflammatory Response with B7-H1 Expression in Human Melanocytic Lesions Supports an Adaptive Resistance Mechanism of Immune Escape. *Science Translational Medicine* 2012;4:127ra137-127ra137.
29. Remon J, Aldea M, Besse B, et al. Small cell lung cancer: a slightly less orphan disease after immunotherapy. *Ann Oncol* 2021.
30. Byers LA, Wang J, Nilsson MB, et al. Proteomic profiling identifies dysregulated pathways in small cell lung cancer and novel therapeutic targets including PARP1. *Cancer*



## Figure Legends

**Figure 1.** Classification of the tumor immune microenvironment on the basis of PD-L1 expression and CD8<sup>+</sup> tumor-infiltrating lymphocyte (TIL) density. (A) Tumor immune microenvironment for 133 small cell lung cancer patients classified according to cutoffs for PD-L1 expression (combined positive score) and CD8<sup>+</sup> TIL density of 1% and the median (85/mm<sup>2</sup>), respectively. Tumors with a PD-L1<sup>positive</sup> and CD8<sup>+</sup> TIL<sup>high</sup> immune microenvironment were designated as inflamed, and all other tumors as noninflamed. (B) Kaplan-Meier curves for progression-free survival of patients with inflamed tumors (n = 7) or noninflamed tumors (n = 56) in the ICI combo-cohort. (C) Kaplan-Meier curves for progression-free survival of patients with inflamed tumors (n = 13) or noninflamed tumors (n = 57) in the chemo-cohort. Abbreviations: CI, confidence interval; NR, not reached; HR, hazard ratio.

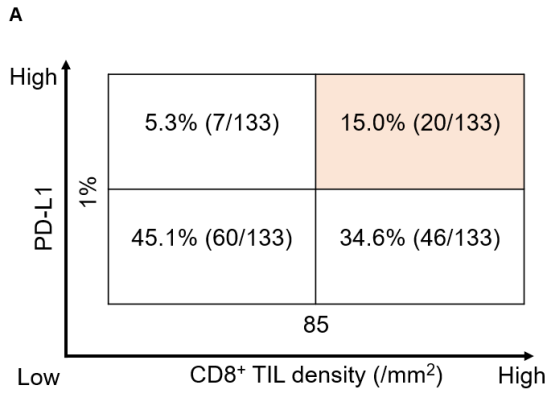
**Figure 2.** Transcriptomic features of the tumor immune microenvironment. (A) Violin plots of the T cell–inflamed gene expression profiling (GEP) score for inflamed tumors (n = 17) and noninflamed tumors (n = 72). The *P* value was determined with the Wilcoxon rank sum test. (B) Heat map of immune-related gene expression in inflamed tumors (n = 17) compared with noninflamed tumors (n = 72). Each colored square represents the Z score for the expression of one gene, with the highest expression shown in red, median in black, and lowest in green. Classification of the tumor immune microenvironment as inflamed or noninflamed is shown above the heat map, and expanded views for selected genes of interest in clusters 1 and 2 that were preferentially expressed in inflamed and noninflamed tumors, respectively, are shown on the right. (C) List of the top 20 and bottom 20 genes expressed differentially in inflamed tumors relative to noninflamed tumors as determined from volcano plot analysis (**Supplementary Fig. S3A**). Genes related to antigen presentation, costimulatory signaling, cytokine and chemokine signaling, cell proliferation, or DNA damage repair are shaded as indicated. FDR, false discovery rate. (D) Violin plots of TIGIT<sup>+</sup> tumor-infiltrating lymphocyte (TIL) density in inflamed (n = 17) and noninflamed (n = 72) tumors. The *P* value was determined with the Wilcoxon rank sum test. (E) Violin plots for the expression of gene signatures related to antigen presentation, cell proliferation, or DNA damage repair in inflamed (n = 17) and noninflamed (n = 72) tumors. The *P* values were determined with the Wilcoxon rank sum test.

**Figure 3.** Genomic features of the tumor immune microenvironment. (A) Violin plots of tumor mutation burden for small cell lung cancer (SCLC) tumors of the present study (n = 85) and for the top 10 and bottom 10 lung adenocarcinoma (LUAD) tumors in The Cancer Genome Atlas (TCGA) ranked according to TMB. The *P* values were determined with Dunn's test, with statistical significance defined as a *P* value of <0.025. (B) Kaplan-Meier curves for progression-free survival according to tumor mutation burden (TMB) in the ICI

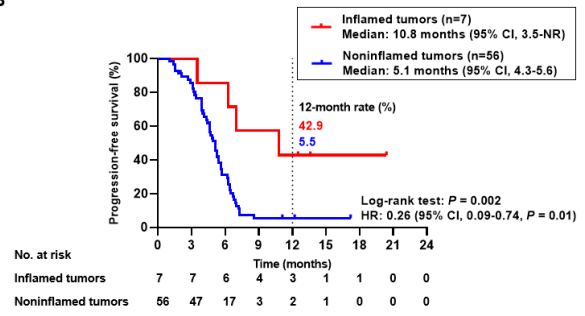
combo-cohort of SCLC patients. Patients were split into high ( $\geq$ median) and low ( $<$ median) TMB groups. CI, confidence interval; HR, hazard ratio. (C) Violin plots for the absolute counts of frameshift insertion-deletion mutations (fs-indels) in SCLC tumors of the present study ( $n = 85$ ) and in the top 10 and bottom 10 LUAD tumors in TCGA ranked according to TMB. The  $P$  values were determined with Dunn's test, with statistical significance defined as a  $P$  value of  $<0.025$ . (D) Violin plots for the proportion of fs-indels in SCLC and LUAD as in (C). (E) Kaplan-Meier curves for progression-free survival according to predicted frameshift neoantigen load in the ICI combo-cohort of SCLC patients. Patients were split into high ( $\geq$ median) and low ( $<$ median) load groups.

**Figure 4.** Classification of small cell lung cancer (SCLC) tumors on the basis of PD-L1 expression, CD8<sup>+</sup> tumor-infiltrating lymphocyte density, immune-related gene expression, and neoantigen status. (A) Change of median gene signature expression in high versus low groups of SCLC tumors ( $n = 55$ ) classified according to the median values for the predicted number of frameshift neoantigens or tumor mutation burden. The change of median gene signature expression is represented by the color scale, with the highest values shown in red, median in white, and lowest in blue. (B) Relation of the predicted number of frameshift neoantigens to the T cell–inflamed gene expression profiling (GEP) score for SCLC tumors ( $n = 55$ ). The  $P$  value was determined with the Spearman correlation test. (C) Kaplan-Meier curves of progression-free survival for the ICI combo-cohort of SCLC patients classified according to inflamed versus noninflamed status as well as predicted frameshift neoantigen load (high defined as  $\geq 5$  frameshift neoantigens per case). Abbreviations: CI, confidence interval; NR, not reached.

Figure 1.



**B**



**C**

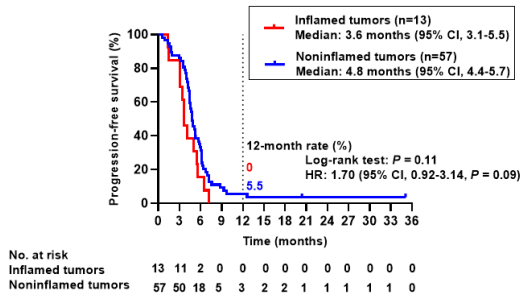
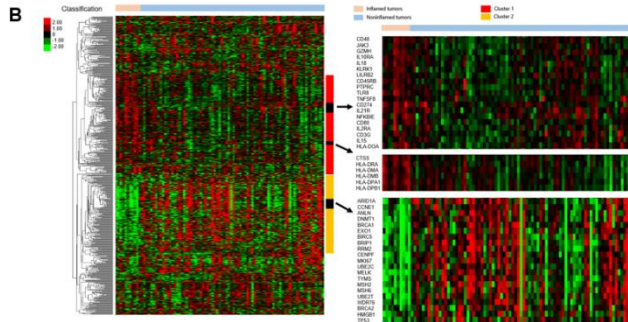
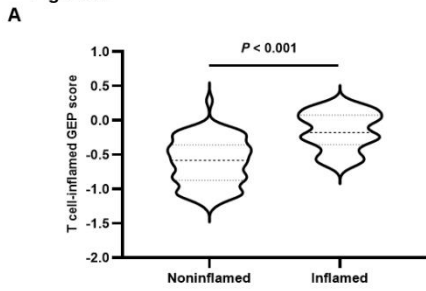


Figure 2.

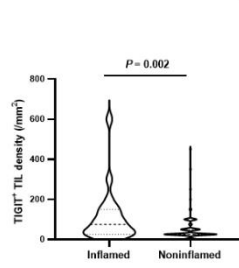


**C**

List of the top 20 genes				List of the bottom 20 genes			
Log2(fold change)	P-value	FDR		Log2(fold change)	P-value	FDR	
TM6SF2	2.04	$3.71 \times 10^{-7}$		SOX11	-2.17	$4.81 \times 10^{-4}$	0.00011
CD8A	2	$7.11 \times 10^{-4}$	0.00209	MHC	-1.22	0.022	0.002
CD8B	1.84	$1.28 \times 10^{-3}$	$3.14 \times 10^{-5}$	ROCK	-1.12	0.038	0.0087
CD8C	1.93	$5.33 \times 10^{-3}$	$3.14 \times 10^{-5}$	NFIB	-1.02	0.0485	0.0186
CD8D	1.93	0.0125	0.0432	CD82	-0.872	0.116	0.217
CD8E	1.9	$3.15 \times 10^{-4}$	0.00007	CD8	-0.86	0.0048	0.0117
CD8F	1.86	$4.40 \times 10^{-3}$	0.00011	CD82L	-0.819	0.0169	0.023
CD8G	1.79	$7.17 \times 10^{-4}$	0.00209	SERPINE5	-0.817	0.0302	0.0041
CD8H	1.76	$1.41 \times 10^{-3}$	$3.14 \times 10^{-5}$	HIT	-0.802	0.0124	0.0037
CD8I	1.77	0.00014	0.0002	NCAM1	-0.778	0.024	0.0074
CD8J	1.7	0.0028	0.027	PDP2	-0.731	0.0248	0.135
CD8K	1.63	0.008	0.107	BDL2	-0.716	0.0123	0.0011
CD8L	1.62	0.00016	0.00123	JAG2	-0.713	0.0157	0.0484
CD8M	1.58	$9.58 \times 10^{-4}$	0.00222	WNT11	-0.678	0.209	0.34
CD8N	1.57	$2.15 \times 10^{-4}$	0.00166	MEZLN1	-0.652	0.0028	0.0026
CD8O	1.54	0.00029	0.00268	PC	-0.648	$4.58 \times 10^{-4}$	0.00011
CD8P	1.52	$3.54 \times 10^{-4}$	0.00168	PC	-0.612	0.0131	0.04
CD8Q	1.52	$1.01 \times 10^{-3}$	0.00229	ORA	-0.607	0.0042	0.0179
CD8R	1.51	0.00014	0.00147	ORA	-0.58	0.12	0.222
CD8S	1.5	0.00108	0.00807	MAPK10	-0.552	0.192	0.323

■ Cytokine and chemokine signaling  
■ Costimulatory signaling  
■ Antigen presentation  
■ Cell proliferation  
■ DNA damage repair

**D**



**E**

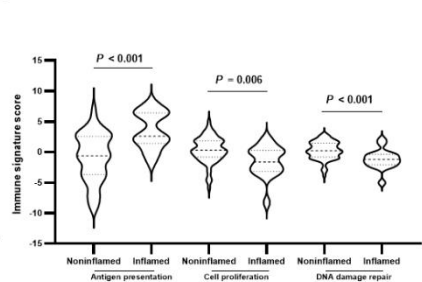


Figure 3.

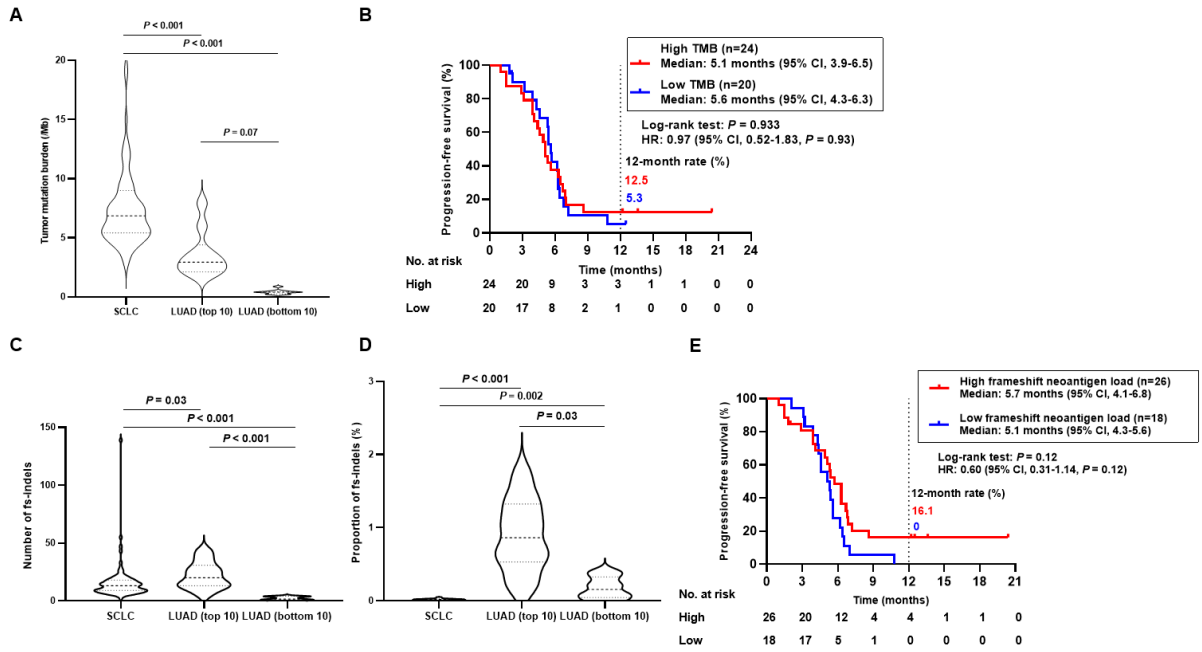
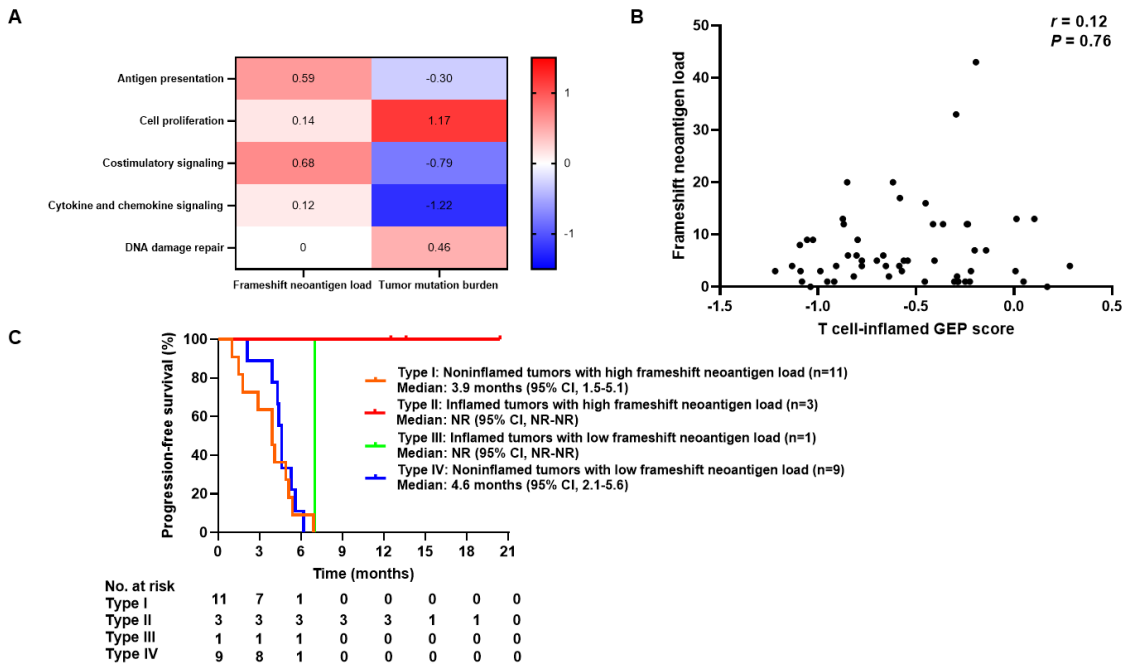


Figure 4.



**Table 1. Characteristics of the Study Patients**

Characteristic	Number of patients (%) <sup>a</sup>		<i>P</i> value <sup>b</sup>
	Chemo-cohort (n=71)	ICI combo-cohort (n=64)	
Median age (range), years <sup>c</sup>	73 (35–84)	72 (34–83)	0.384
Sex			
Male	55 (77.5)	53 (82.8)	0.520
Female	16 (22.5)	11 (17.2)	
ECOG performance status			
0–1	54 (76.1)	55 (85.9)	0.293
2	12 (16.9)	5 (7.8)	
3–4	5 (7.0)	4 (6.3)	
Smoking status <sup>d</sup>			
Current or former	68 (95.8)	63 (98.4)	0.687
Never	2 (2.8)	1 (1.6)	
Unknown	1 (1.4)	0 (0)	
Stage			
Limited	8 (11.3)	4 (6.3)	0.374
Extensive	63 (88.7)	60 (93.8)	
Metastasis at baseline			
CNS	17 (23.9)	20 (31.2)	0.440
Intrathoracic only	9 (12.7)	9 (14.1)	1.00
Extrathoracic	54 (76.1)	52 (81.3)	0.532
Histology			
Small cell	66 (93.0)	61 (95.3)	0.721
Combined	5 (7.0)	3 (4.7)	
Treatment			
Surgery	9 (12.7)	4 (6.3)	0.252
Radiotherapy	4 (5.6)	6 (9.4)	0.517
PD-L1 TPS (22C3)			
≥1%	3 (4.2)	3 (4.7)	1.00
<1%	68 (95.8)	61 (95.3)	
PD-L1 CPS (22C3)			
≥1%	18 (25.4)	9 (14.1)	0.132
<1%	53 (74.6)	55 (85.9)	

Abbreviations: ECOG, Eastern Cooperative Oncology Group; CNS, central nervous system; TPS, tumor proportion score; CPS, combined positive score.

<sup>a</sup>Percentages may not add up to 100 because of rounding.

<sup>b</sup>*P* values were determined with the Wilcoxon rank sum test or Fisher's exact test as appropriate.

<sup>c</sup>At the start of treatment.

<sup>d</sup>Current smokers, individuals who had smoked a cigarette within the previous year; former smokers, those who had smoked ≥100 cigarettes but had quit >1 year before diagnosis; never-smokers, those who had smoked <100 cigarettes.

**Table 2. Predicted Neoantigens for SCLC (This Study) and LUAD (TCGA)**

	Mutations (n)	Neoantigens (n)	Neoantigens per mutation
SCLC (n=85)			
nsSNVs	21,059	3299	0.16
fs-indels	1346	662	0.49
fs-indel enrichment			3.14
LUAD (top 10 for TMB)			
nsSNVs	1013	118	0.12
fs-indels	219	132	0.60
fs-indel enrichment			5.17
LUAD (bottom 10 for TMB)			
nsSNVs	38	3	0.08
fs-indels	20	47	2.35
fs-indel enrichment			29.8

SCLC, small cell lung cancer; LUAD, lung adenocarcinoma; TCGA, The Cancer Genome Atlas; nsSNVs, nonsynonymous single nucleotide variants; fs-indels, frameshift insertions and deletions; TMB tumor mutation burden.

## Supplementary Methods

### Immunohistochemistry

Tumor histology was classified according to WHO criteria.<sup>1</sup> Sections of formalin-fixed paraffin-embedded (FFPE) tumor tissue (thickness, 4  $\mu\text{m}$ ) from patients in the IHC biomarker analysis set were subjected to immunohistochemistry (IHC) with monoclonal antibodies to PD-L1 (kit with clone 22C3, Agilent Technologies), to CD8 (clone C8/144B, Agilent Technologies), and to TIGIT (clone TG1, Oncodiana) and with the use of an automated stainer (Autostainer Link 48 and Leica Bond-Max). The stained slides were evaluated by a board-certified pathologist who was blinded to clinical outcome.

PD-L1 immunostaining was optimized with human placenta and tonsil as positive controls. The percentage of tumor cells positive for PD-L1 was determined as the PD-L1 tumor proportion score (TPS).<sup>2,3</sup> The combined positive score (CPS) for PD-L1 expression was also calculated as the number of PD-L1-positive cells (tumor cells, lymphocytes, macrophages) divided by the total number of tumor cells and multiplied by 100.<sup>4,5</sup> PD-L1 positivity was defined as membranous staining at any intensity with a cutoff of  $\geq 1\%$  of tumor cells ( $< 1\%$  defined as negative).

Tumor-infiltrating lymphocytes (TILs) were evaluated on the basis of staining for CD8 and TIGIT. Tumor tissue samples including at least 100 viable tumor cells were eligible for TIL assessment. The number of TILs was determined at an absolute magnification of  $400\times$  ( $0.20\text{ mm}^2$  per field). At least one and a maximum of five scanned fields of tumor regions were randomly chosen for each TIL count. TILs were counted by a board-certified pathologist, and the density of TILs in each tumor was calculated by dividing the number of TILs by the sum of the area ( $\text{mm}^2$ ) of the viewed fields.<sup>3</sup> TILs were defined as cells positive for CD8 or TIGIT at any staining intensity.

### Immune-related gene expression profiling

Immune-related gene expression profiling (irGEP) was performed with RNA isolated from baseline FFPE tumor samples. Sections were first examined by hematoxylin-eosin staining to confirm the presence of invasive tumor cells and to determine the tumor area. Macrodissection was performed when needed to avoid contamination with normal tissue. Tissue obtained by transbronchial needle aspiration and cell block specimens were excluded to avoid contamination by non-tumor-infiltrating immune cells. Total RNA was extracted from the dissected FFPE tumor tissue with the use of an AllPrep DNA/RNA FFPE Kit (Qiagen). The amount of extracted RNA was measured with a NanoDrop 2000 device (Thermo Fisher Scientific) and Ribogreen RNA Assay Kit (Thermo Fisher Scientific). The integrity of the RNA was assessed with an Agilent RNA 6000 Nano Kit and an Agilent 2100 Bioanalyzer (Agilent Technologies), and the percentage of fragments comprising  $\geq 300$  nucleotides (DV300) was calculated. A minimum of 50 ng of total RNA was used for gene expression analysis with the nCounter platform and a PanCancer IO 360 Gene Expression Panel comprising 750 immune-related genes and 20 housekeeping genes (NanoString Technologies). Tumor-derived RNA obtained from 95 patients was thus analyzed. Gene expression was normalized on the basis of the data for the 20 housekeeping genes with the use of nSolver Analysis Software 4.0 and nCounter Advanced Analysis 2.0 (NanoString Technologies). Samples with abnormal normalized expression values (normalization factor of  $> 10$  obtained with nSolver Analysis Software 4.0) were excluded, in accordance with the manufacturer's instructions. A total of 89 RNA samples thus remained for further analysis. Of the 750 immune-related genes analyzed, 74 genes for which  $> 60\%$  of samples showed an expression value below the minimum threshold were filtered out. The normalized gene expression data were  $\log_2$ -transformed before calculation of the Z score. Gene clustering was performed with the use of Cluster3.0 software, and a heat map was constructed with the use

of Java TreeView.<sup>6</sup>

The T cell–inflamed GEP score was based on the expression of 18 inflammatory genes related to antigen presentation, chemokine expression, cytolytic activity, and adaptive immune resistance: *CCL5*, *CD27*, *CD274* (*PD-L1*), *CD276* (*B7-H3*), *CD8A*, *CMKLR1*, *CXCL9*, *CXCR6*, *HLA-DQA1*, *HLA-DQB1*, *HLA-E*, *IDO1*, *LAG3*, *NKG7*, *PDCD1LG2* (*PD-L2*), *PSMB10*, *STAT1*, *TIGIT*. The score was calculated as the weighted sum of the normalized expression values for these 18 genes.<sup>7, 8</sup>

Immune signatures representative of 11 immune cell types and 25 immune-related pathways were curated as in previous studies.<sup>9-11</sup> The cell type signatures and corresponding genes were as follows. Cytotoxic cells (7 genes): *NKG7*, *KLRK1*, *PRF1*, *GZMA*, *KLRD1*, *KLRB1*, *GNLY*. Macrophages (4 genes): *CD68*, *CD84*, *MS4A4A*, *CD163*. Dendritic cells (2 genes): *CD209*, *HSD11B1*. Exhausted CD8 cells (3 genes): *LAG3*, *EOMES*, *PTGER4*. B cells (5 genes): *TNFRSF17*, *MS4A1*, *CD19*, *SPIB*, *FAM30A*. CD45 cells (3 genes): *CD45RA*, *PTPRC*, *CD45RO*. Neutrophils (4 genes): *FPR1*, *FCGR3A/B*, *CSF3R*, *CEACAM3*. T cells (5 genes): *TRAT1*, *CD3D*, *CD6*, *CD3E*, *SH2D1A*. Mast cells (2 genes): *TPSAB1/B2*, *CPA3*. CD8 T cells (2 genes): *CD8A*, *CD8B*. Natural killer cells (1 gene): *XCL1/2*. The pathway signatures and corresponding genes were as follows: Angiogenesis (35 genes): *ANGPT1*, *ANGPT2*, *ANGPTL4*, *CCND2*, *CCNE1*, *CES3*, *DLL4*, *E2F3*, *EDN1*, *EZH2*, *FGF18*, *FGFR1*, *FLT1*, *FSTL3*, *HEY1*, *ITGAV*, *ITPK1*, *JAG1*, *MMP9*, *MMRN2*, *NFIL3*, *PDGFB*, *PGPEP1*, *RPL7A*, *SERPINB5*, *SERPINH1*, *STC1*, *THBS1*, *TNFAIP6*, *TPM1*, *TYMP*, *VCAN*, *VEGFA*, *VEGFB*, *VEGFC*. Antigen presentation (51 genes): *ATF3*, *B2M*, *BATF3*, *CCL4*, *CCR5*, *CD36*, *CD4*, *CD74*, *CD8A*, *CD8B*, *CDC20*, *CTSS*, *CXCL1*, *CYBB*, *DTX3L*, *FCGR1A*, *HLA-A*, *HLA-B*, *HLA-C*, *HLA-DMA*, *HLA-DMB*, *HLA-DOA*, *HLA-DOB*, *HLA-DPA1*, *HLA-DPBI*, *HLA-DQA1*, *HLA-DQB1*, *HLA-DRA*, *HLA-DRB1*, *HLA-E*, *HLA-F*, *IRF8*, *ITGAV*, *KIF2C*, *KLRD1*, *MRC1*, *PSMB10*, *PSMB5*, *PSMB8*, *PSMB9*, *SOCS1*, *TAP1*, *TAP2*, *TAPBP*, *THBD*, *TNF*, *TRIM21*, *UBA7*, *UBE2C*, *ULBP2*, *VHL*. Apoptosis (34 genes): *AKT1*, *APC*, *BAD*, *BAX*, *BBC3*, *BCL2*, *BCL2L1*, *BCL6B*, *BID*, *BIRC5*, *BLM*, *CASP1*, *CASP3*, *CASP8*, *CASP9*, *CD14*, *CDH1*, *CTNNB1*, *FADD*, *HMGB1*, *LY96*, *PSMB10*, *PSMB5*, *PSMB8*, *PSMB9*, *RIPK1*, *RIPK3*, *ROCK1*, *TICAM1*, *TLR3*, *TLR4*, *TNFRSF10B*, *TNFSF10*, *TP53*. Autophagy (23 genes): *AKT1*, *BAD*, *BCL2*, *BCL2L1*, *BNIP3*, *DEPTOR*, *HIF1A*, *HMGB1*, *HRAS*, *KRAS*, *MAP3K7*, *MAPK10*, *MTOR*, *NRAS*, *PIK3CA*, *PIK3CD*, *PIK3R1*, *PIK3R2*, *PRKAA2*, *PRKACB*, *PTEN*, *RPS6KB1*, *RPTOR*. Cell proliferation (48 genes): *ANLN*, *ATM*, *BIRC5*, *BLM*, *BRCA1*, *BRCA2*, *CCNA1*, *CCNB1*, *CCND1*, *CCND2*, *CCND3*, *CCNE1*, *CCNO*, *CDC20*, *CDC25C*, *CDK2*, *CDK6*, *CDKN1A*, *CDKN1C*, *CDKN2A*, *CDKN2B*, *CENPF*, *CEP55*, *E2F3*, *EXO1*, *H2AFX*, *KIF2C*, *MELK*, *MKI67*, *MLH1*, *MYC*, *NBN*, *PIAS4*, *POLD1*, *PRKCA*, *PSMB10*, *PSMB5*, *PSMB8*, *PSMB9*, *RAD50*, *RAD51*, *RAD51C*, *RB1*, *RBL2*, *RRM2*, *TP53*, *TYMS*, *UBE2C*. Costimulatory signaling (73 genes): *ADORA2A*, *AKT1*, *CD2*, *CD247*, *CD27*, *CD274*, *CD28*, *CD3D*, *CD3E*, *CD4*, *CD40*, *CD44*, *CD48*, *CD69*, *CD80*, *CD86*, *CHUK*, *CTLA4*, *DPP4*, *EGR1*, *FYN*, *HAVCR2*, *HLA-DPA1*, *HLA-DPBI*, *HLA-DQA1*, *HLA-DQB1*, *HLA-DRA*, *HLA-DRB1*, *ICOSLG*, *IKBKB*, *IKBKG*, *IL15*, *IL18*, *IL18R1*, *IL2RA*, *IL2RB*, *IL2RG*, *LAG3*, *LCK*, *LILRB2*, *MAP3K7*, *MAP3K8*, *MTOR*, *NECTIN2*, *NFATC2*, *NFKB1*, *NFKBIA*, *PDCD1LG2*, *PIK3CA*, *PIK3R1*, *PIK3R2*, *PRR5*, *PSMB10*, *PSMB5*, *PSMB8*, *PSMB9*, *PTEN*, *PTGS2*, *PTPN11*, *PTPRC*, *PVRIG*, *RELA*, *RICTOR*, *RIPK2*, *SPP1*, *STAT4*, *TIGIT*, *TNFRSF14*, *TNFRSF25*, *TRAT1*, *TSLP*, *VTCN1*, *ZAP70*. Cytokine and chemokine signaling (80 genes): *AKT1*, *CCL14*, *CCL18*, *CCL19*, *CCL2*, *CCL20*, *CCL21*, *CCL3/L1*, *CCL4*, *CCL5*, *CCL8*, *CCR2*, *CCR4*, *CCR5*, *CHUK*, *CSF1*, *CSF1R*, *CSF2RB*, *CSF3R*, *CX3CL1*, *CX3CR1*, *CXCL1*, *CXCL10*, *CXCL12*, *CXCL13*, *CXCL14*, *CXCL16*, *CXCL2*, *CXCL3*, *CXCL6*, *CXCL8*, *CXCL9*, *CXCR2*, *CXCR4*, *CXCR6*, *GNG4*, *HCK*, *HRAS*, *IKBKB*, *IKBKG*, *IL10RA*, *IL11*, *IL11RA*, *IL12RB2*, *IL15*, *IL16*, *IL18*, *IL18R1*, *IL1A*, *IL1B*, *IL1R2*, *IL22RA1*, *IL2RA*, *IL2RB*, *IL2RG*, *IL32*, *IL33*, *IL34*, *IL6*, *IL6R*, *IL7R*, *JAK2*, *JAK3*, *KRAS*, *NFKB1*, *NFKBIA*, *NRAS*, *PIK3CA*, *PIK3CD*, *PIK3CG*, *PIK3R1*, *PIK3R2*, *PIK3R5*,

PRKACB, RELA, ROCK1, SHC2, STAT1, STAT2, STAT3. Cytotoxicity (42 genes): BBC3, CBLC, CD47, GHR, GNLY, GZMA, GZMK, IFI16, IFI27, IFI35, IFI6, IFIH1, IFIT1, IFIT2, IFIT3, IFITM1, IFITM2, IGF2R, IL11RA, IL12RB2, IL22RA1, IRF1, IRF4, IRF9, ISG15, JAK1, JAK2, JAK3, KLRB1, KLRD1, KLRK1, LIF, MX1, OAS1, OAS2, OAS3, PRF1, SIRPA, SPRY4, STAT1, STAT2, TNFSF10. DNA damage repair (31 genes): ATM, BLM, BRCA1, BRCA2, BRIP1, CCNA1, CCNO, CDK2, DDB2, EXO1, FANCA, H2AFX, ISG15, MGMT, MLH1, MSH2, MSH6, NBN, NEIL1, PARP4, PIAS4, PMS2, POLD1, RAD50, RAD51, RAD51C, TNKS, TP53, UBA7, UBE2T, XCL1/2. Epigenetic regulation (17 genes): ARID1A, BNIP3, BRD3, BRD4, CCND1, DNMT1, EZH2, H2AFX, HDAC11, HDAC3, HDAC4, HDAC5, HELLS, HMGA1, JAK2, KAT2B, MAP3K12. Hedgehog signaling (14 genes): BMP2, GAS1, GLI1, PRKACB, PSMB10, PSMB5, PSMB8, PSMB9, WNT10A, WNT11, WNT2B, WNT5A, WNT5B, WNT7B. Hypoxia (39 genes): AKT1, ALDOA, ANGPT1, ANGPT2, BCL2, CDKN1A, CYBB, EDN1, EGFR, EIF4EBP1, ENO1, ERBB2, FLT1, HIF1A, HK1, HK2, IFNGR1, IFNGR2, IL6, IL6R, LDHA, MTOR, NFKB1, PDK1, PFKFB3, PIK3CA, PIK3CD, PIK3CG, PIK3R1, PIK3R2, PIK3R5, PRKCA, RELA, RPS6KB1, SLC2A1, STAT3, TLR4, VEGFA, VHL. Immune cell adhesion and migration (80 genes): CD2, CD274, CD276, CD28, CD4, CD40, CD58, CD6, CD80, CD86, CD8A, CD8B, CDH1, CDH2, CDH5, CLEC14A, CLEC7A, CLECL1, CTLA4, CTNNB1, CXCL12, CXCR4, CYBB, HLA-A, HLA-B, HLA-C, HLA-DMA, HLA-DMB, HLA-DOA, HLA-DOB, HLA-DPA1, HLA-DPB1, HLA-DQA1, HLA-DQB1, HLA-DRA, HLA-DRB1, HLA-E, HLA-F, ICAM1, ICAM2, ICAM3, ICOSLG, ITGA1, ITGA2, ITGA4, ITGA6, ITGAE, ITGAL, ITGAM, ITGAV, ITGAX, ITGB2, ITGB3, ITGB8, MMP9, NCAM1, NECTIN1, NECTIN2, PDCD1LG2, PECAM1, PIK3CA, PIK3CD, PIK3CG, PIK3R1, PIK3R2, PIK3R5, PRKCA, PTPN11, PTPRC, PVR, ROCK1, SELE, SELL, SELP, SIGLEC1, THY1, TIGIT, VCAM1, VCAN, VTCN1. Interferon signaling (62 genes): B2M, CD44, EGR1, EIF2AK2, FCGR1A, FLNB, GBP1, GBP2, GBP4, GHR, HLA-A, HLA-B, HLA-C, HLA-DPA1, HLA-DPB1, HLA-DQA1, HLA-DQB1, HLA-DRA, HLA-DRB1, HLA-E, HLA-F, ICAM1, IFI16, IFI27, IFI35, IFI6, IFIH1, IFIT1, IFIT2, IFIT3, IFITM1, IFITM2, IFNAR1, IFNGR1, IFNGR2, IGF2R, IRF1, IRF2, IRF3, IRF4, IRF5, IRF7, IRF8, IRF9, ISG15, JAK1, JAK2, MX1, NCAM1, OAS1, OAS2, OAS3, OASL, PSMB8, PTPN11, RSAD2, SOCS1, STAT1, STAT2, TRIM21, UBA7, VCAM1. JAK-STAT signaling (47 genes): AKT1, BCL2, BCL2L1, CCND1, CCND2, CCND3, CDKN1A, CSF2RB, CSF3R, GHR, HRAS, IFNAR1, IFNGR1, IFNGR2, IL10RA, IL11, IL11RA, IL12RB2, IL15, IL22RA1, IL2RA, IL2RB, IL2RG, IL6, IL6R, IL7R, IRF9, JAK1, JAK2, JAK3, LIF, MTOR, MYC, PIAS4, PIK3CA, PIK3CD, PIK3CG, PIK3R1, PIK3R2, PIK3R5, PTPN11, SOCS1, STAT1, STAT2, STAT3, STAT4, TSLP. Lymphoid compartment (65 genes): CCR4, CD19, CD2, CD27, CD274, CD28, CD38, CD3D, CD3E, CD40, CD48, CD5, CD6, CD7, CD79A, CD80, CD86, CD8A, CD8B, CD96, CTLA4, CX3CL1, CXCL10, CXCL13, CXCL16, CXCL9, DPP4, EGR1, EOMES, F2RL1, GNLY, GZMA, GZMK, HLA-DOB, ICOSLG, IDO1, IFI27, IFIT1, IFITM1, IGF2R, IL11, IL12RB2, IL18R1, IL2RG, IRF4, IRF9, ISG15, ITGA1, JAK1, JAK2, KLRB1, KLRD1, KLRK1, LAG3, LCK, MS4A1, MX1, PRF1, PVR, SLAMF7, STAT1, STAT2, TIGIT, TNFRSF25, ZAP70. MAPK (72 genes): AKT1, ANGPT1, ANGPT2, BAD, BCL2L1, CASP3, CD14, CHUK, CSF1, CSF1R, DUSP1, DUSP2, DUSP5, EGFR, FAS, FGF13, FGF18, FGF9, FGFR1, FLNB, FLT1, GNG4, HRAS, IKBKB, IKBKG, IL1A, IL1B, IL1R2, KDR, KIT, KRAS, MAP3K12, MAP3K5, MAP3K7, MAP3K8, MAPK10, MET, MYC, NF1, NFKB1, NFKB2, NGFR, NRAS, PDGFA, PDGFB, PDGFRB, PIK3CA, PIK3CD, PIK3CG, PIK3R1, PIK3R2, PIK3R5, PLA1A, PRKACB, PRKCA, PTPN11, RASAL1, RELA, RELB, SHC2, TGFB1, TGFB2, TGFB3, TGFBRI, TGFBRII, TNF, TNFRSF1A, TP53, VEGFA, VEGFB, VEGFC, ZAP70. Matrix remodeling and metastasis (54 genes): A2M, BMP2, CASP3, CD36, CD44, CD47, CDH1, COL11A1, COL17A1, COL4A5, COL5A1, COL6A3, COMP, CTSS, ICAM1, ICAM2, ICAM3, ITGA1, ITGA2, ITGA4, ITGA6, ITGAE, ITGAL, ITGAM, ITGAV, ITGAX, ITGB2, ITGB3, ITGB8, KDR, LAMA1, LAMB3, LAMC2,

*LOXL2, LTBP1, MMP1, MMP7, MMP9, NCAM1, NID2, PDGFA, PDGFB, PECAM1, PLOD2, PRKCA, RELN, SERPINH1, SPP1, TGFB1, TGFB2, TGFB3, THBS1, VCAM1, VCAN.* Metabolic stress (82 genes): *AKT1, AQP9, ATM, CCNA1, CCNE1, CD300A, CDK2, CDK6, CDKN1A, CDKN2A, CDKN2B, CEBPB, CXCL8, DEPTOR, E2F3, EGFR, EIF4EBP1, ENO1, ERBB2, ERO1A, EZH2, FBP1, FGFR1, GLS, GOT1, GOT2, H2AFX, HIF1A, HK1, HK2, HMGA1, HRAS, IKBKB, IL1A, IL6, KIT, KRAS, LDHA, LDHB, MAP3K5, MAPK10, MET, MTOR, MYC, NBN, NFKB1, NRAS, PC, PCK2, PDGFRB, PDK1, PFKFB3, PFKM, PIK3CA, PIK3CD, PIK3CG, PIK3R1, PIK3R2, PIK3R5, PKM, PRKAA2, PRKCA, PRR5, PTEN, RAD50, RB1, RELA, RICTOR, RPS6KB1, RPTOR, SGK1, SLC16A1, SLC1A5, SLC2A1, SLC7A5, STAT3, TNF, TP53, TPI1, UBE2C, VEGFA, VHL.* Myeloid compartment (63 genes): *ANGPT1, C5AR1, CCL2, CCL20, CCL4, CCL5, CCL8, CD14, CD47, CDKN1A, CEBPB, CLEC7A, COL11A1, COL17A1, CRABP2, CSF1, CSF1R, CSF3R, CXCL1, CXCL12, CXCL2, CXCL3, CXCL6, CYBB, DAB2, DLL4, FCGR1A, FCN1, FOSL1, FPR1, FPR3, HCK, IER3, IL1A, IL1B, ITGAM, ITGAX, LAMB3, LIF, LILRA5, LILRB2, LY96, LYZ, MMP1, MRC1, NFAM1, NLRP3, P2RY13, PDZK1IP1, PTGS2, S100A8, S100A9, SERPINA1, SIRPA, SIRPB2, SLC11A1, TLR1, TLR2, TLR4, TLR8, TNFAIP6, TREM1, TREM2.* NF- $\kappa$ B signaling (31 genes): *CD27, CD40, CHUK, IKBKB, IKBKG, LTB, NFKB1, NFKB2, NFKBIA, NFKBIE, PSMB10, PSMB5, PSMB8, PSMB9, RELA, RELB, RELN, TNF, TNFRSF11A, TNFRSF11B, TNFRSF14, TNFRSF17, TNFRSF18, TNFRSF1A, TNFRSF1B, TNFRSF25, TNFRSF4, TNFSF12, TNFSF13, TNFSF13B, TNFSF4.* Notch signaling (23 genes): *APH1B, CCND1, DLL1, DLL4, DTX3L, DTX4, E2F3, HDAC11, HDAC3, HDAC4, HDAC5, HES1, HEY1, HIF1A, JAG1, JAG2, KAT2B, MAML2, MFNG, MYC, NOTCH1, NOTCH2, TP53.* PI3K-Akt (92 genes): *AKT1, ANGPT1, ANGPT2, BAD, BCL2, BCL2L1, BRCA1, CASP9, CCND1, CCND2, CCND3, CCNE1, CD19, CDK2, CDK6, CDKN1A, CHUK, COL4A5, COL6A3, COMP, CSF1, CSF1R, CSF3R, EGFR, EIF4EBP1, FGF13, FGF18, FGF9, FGFR1, FLT1, GHR, GNG4, HRAS, IFNAR1, IKBKB, IKBKG, IL2RA, IL2RB, IL2RG, IL6, IL6R, IL7R, ITGA1, ITGA2, ITGA4, ITGA6, ITGAV, ITGB3, ITGB8, JAK1, JAK2, JAK3, KDR, KIT, KRAS, LAMA1, LAMB3, LAMC2, MET, MTOR, MYC, NFKB1, NGFR, NRAS, PCK2, PDGFA, PDGFB, PDGFRB, PIK3CA, PIK3CD, PIK3CG, PIK3R1, PIK3R2, PIK3R5, PRKAA2, PRKCA, PTEN, RBL2, RELA, RELN, RPS6KB1, RPTOR, SGK1, SPP1, SYK, THBS1, TLR2, TLR4, TP53, VEGFA, VEGFB, VEGFC.* TGF- $\beta$  signaling (19 genes): *ACVR1C, BAMBI, BMP2, CDKN2B, ID4, INHBA, LTBP1, MYC, RBL2, ROCK1, RPS6KB1, SMAD5, TGFB1, TGFB2, TGFB3, TGFBRI, TGFBRII, THBS1, TNF.* Wnt signaling (29 genes): *APC, AXIN1, BAMBI, CCND1, CCND2, CCND3, CTNNB1, FOSL1, FZD8, FZD9, GPC4, MAP3K7, MAPK10, MMP7, MYC, NFATC2, PRKACB, PRKCA, SFRP1, SFRP4, SOX11, SOX2, TP53, WNT10A, WNT11, WNT2B, WNT5A, WNT5B, WNT7B.*

### **Whole-Exome Sequencing and Exome Analysis Pipeline**

Whole-exome sequencing (WES) was performed to evaluate tumor mutation burden (TMB) in 41 and 44 tumor samples obtained from the chemo-cohort and ICI combo-cohort, respectively. TMB was broadly defined as the total number of SNVs (both synonymous and nonsynonymous) and indels per tumor genomic region analyzed. DNA was extracted from FFPE tumor specimens with the use of an AllPrep DNA/RNA FFPE Kit (Qiagen), and its quality and quantity were determined with the use of a NanoDrop 2000 device (Thermo Fisher Scientific) and PicoGreen dsDNA Assay Kit (Thermo Fisher Scientific). Integrity was assessed on the basis of the DNA Integrity Number (DIN) measured with the Agilent 2200 TapeStation system (Agilent Technologies). Samples for which the concentration of extracted DNA was <10 ng/ $\mu$ L or the DIN was <4.5 were excluded from the analysis. Whole-exome capture libraries were constructed with the use of an Agilent Sure-Select Human All Exon v7.0 system (Agilent Technologies), with the capture region being 48.2 Mb. Samples with a

library concentration of >20 ng/μL were used for further analysis. Enriched exome libraries were sequenced with the NovaSeq 6000 platform (Illumina), yielding an average of 68 million reads (10 Gb). Somatic mutations were identified with SAMtools<sup>12</sup> and the Ensemble Variant Effect Predictor (VEP) pipeline.<sup>13</sup> In brief, the *identify-and-annotate-variants* workflow was applied for mapping to the reference genome (hg38), identification of variants, and annotation. The *filter-somatic-variants* and *remove-variants-outside-genome-regions* workflows were then applied to remove variants outside the target (coding) regions and common variants present in publicly available databases. Sorting Tolerant From Intolerant (SIFT)<sup>14, 15</sup> and Polymorphism Phenotyping v2 (PolyPhen-2) scores were obtained from VEP.<sup>13</sup> Filtered mutations were evaluated as deleterious if denoted as such by both SIFT (“deleterious”) and PolyPhen-2 (“damaging”) or VEP IMPACT (high or low). SNV and indel mutation counts were computed per case. We performed the same analysis for our SCLC cohort and the lung adenocarcinoma (LUAD) data set from The Cancer Genome Atlas (TCGA).

### **Neoantigen Prediction Workflow**

Human leukocyte antigen (HLA) genotypes were determined from the WES data for each patient with the use of HLAScan.<sup>16</sup> HLAScan identified the four-digit HLA type as well as mutations in HLA class I genes for each sample. Mutant peptides were computed on the basis of the nsSNV and indel mutations with the use of SeqTailor.<sup>17</sup> Peptide-MHC binding affinities were predicted with the use of NetMHCpan (version 4.0).<sup>18</sup> Representative antigens with a binding affinity of <50 nM for HLA-A, -B, or -C were considered neoantigens.<sup>8, 19</sup> We performed the same analysis for our SCLC cohort and the LUAD data set of TCGA.

### **TCGA Molecular Data**

Somatic alteration data for 20 LUAD samples (top 10 and bottom 10 TMB samples) were obtained through TCGA Genomic Data Commons Data Portal as of July 2021. These samples were analyzed for TMB and predicted neoantigen burden by the same bioinformatics pipelines as those applied for our SCLC cohort.

## References

1. Travis WD, Brambilla E, Nicholson AG, et al. The 2015 World Health Organization Classification of Lung Tumors: Impact of Genetic, Clinical and Radiologic Advances Since the 2004 Classification. *J Thorac Oncol* 2015;10:1243-1260.
2. Borghaei H, Paz-Ares L, Horn L, et al. Nivolumab versus Docetaxel in Advanced Nonsquamous Non-Small-Cell Lung Cancer. *N Engl J Med* 2015;373:1627-1639.
3. Haratani K, Hayashi H, Tanaka T, et al. Tumor immune microenvironment and nivolumab efficacy in EGFR mutation-positive non-small-cell lung cancer based on T790M status after disease progression during EGFR-TKI treatment. *Ann Oncol* 2017;28:1532-1539.
4. Kulangara K, Zhang N, Corigliano E, et al. Clinical Utility of the Combined Positive Score for Programmed Death Ligand-1 Expression and the Approval of Pembrolizumab for Treatment of Gastric Cancer. *Arch Pathol Lab Med* 2019;143:330-337.
5. Ott PA, Bang YJ, Piha-Paul SA, et al. T-Cell-Inflamed Gene-Expression Profile, Programmed Death Ligand 1 Expression, and Tumor Mutational Burden Predict Efficacy in Patients Treated With Pembrolizumab Across 20 Cancers: KEYNOTE-028. *J Clin Oncol* 2019;37:318-327.
6. Haratani K, Hayashi H, Takahama T, et al. Clinical and immune profiling for cancer of unknown primary site. *J Immunother Cancer* 2019;7:251.
7. Ayers M, Lunceford J, Nebozhyn M, et al. IFN-gamma-related mRNA profile predicts clinical response to PD-1 blockade. *J Clin Invest* 2017;127:2930-2940.
8. Cristescu R, Mogg R, Ayers M, et al. Pan-tumor genomic biomarkers for PD-1 checkpoint blockade-based immunotherapy. *Science* 2018;362.
9. Tomfohr J, Lu J, Kepler TB. Pathway level analysis of gene expression using singular value decomposition. *BMC Bioinformatics* 2005;6:225.
10. Danaher P, Warren S, Lu R, et al. Pan-cancer adaptive immune resistance as defined by the Tumor Inflammation Signature (TIS): results from The Cancer Genome Atlas (TCGA). *J Immunother Cancer* 2018;6:63.
11. Bindea G, Mlecnik B, Tosolini M, et al. Spatiotemporal dynamics of intratumoral immune cells reveal the immune landscape in human cancer. *Immunity* 2013;39:782-795.
12. Danecek P, Bonfield JK, Liddle J, et al. Twelve years of SAMtools and BCFtools. *Gigascience* 2021;10.
13. McLaren W, Gil L, Hunt SE, et al. The Ensembl Variant Effect Predictor. *Genome Biol* 2016;17:122.
14. Kumar P, Henikoff S, Ng PC. Predicting the effects of coding non-synonymous variants on protein function using the SIFT algorithm. *Nature Protocols* 2009;4:1073-1081.
15. Ng PC, Henikoff S. SIFT: predicting amino acid changes that affect protein function. *Nucleic Acids Research* 2003;31:3812-3814.
16. Ka S, Lee S, Hong J, et al. HLAscan: genotyping of the HLA region using next-generation sequencing data. *BMC Bioinformatics* 2017;18:258.
17. Zhang P, Boisson B, Stenson PD, et al. SeqTailor: a user-friendly webserver for the extraction of DNA or protein sequences from next-generation sequencing data. *Nucleic Acids Res* 2019;47:W623-W631.
18. Jurtz V, Paul S, Andreatta M, et al. NetMHCpan-4.0: Improved Peptide-MHC Class I Interaction Predictions Integrating Eluted Ligand and Peptide Binding Affinity Data. *J Immunol* 2017;199:3360-3368.
19. Turajlic S, Litchfield K, Xu H, et al. Insertion-and-deletion-derived tumour-specific neoantigens and the immunogenic phenotype: a pan-cancer analysis. *The Lancet Oncology* 2017;18:1009-1021.

## Supplementary Figures

**Supplementary Figure S1.** Flow of the study patients with extensive-stage small cell lung cancer. Abbreviations: ICI, immune checkpoint inhibitor; IHC, immunohistochemistry; WES, whole-exome sequencing; irGEP, immune-related gene expression profiling; EBUS-TBNA, endobronchial ultrasound with transbronchial needle aspiration.

**Supplementary Figure S2.** Kaplan-Meier curves for progression-free survival in the chemo-cohort (A) and ICI combo-cohort (B). Abbreviation: CI, confidence interval.

**Supplementary Figure S3.** Transcriptomic features of inflamed and noninflamed tumors. (A) Differential gene expression analysis for inflamed tumors ( $n = 17$ ) and noninflamed tumors ( $n = 72$ ). Benjamini-Hochberg adjusted  $P$  ( $P_{adj}$ ) values are color coded. (B) Relation between TIGIT gene expression and TIGIT<sup>+</sup> tumor-infiltrating lymphocyte (TIL) density in SCLC tumors ( $n = 89$ ). The  $P$  value was determined with the Spearman correlation test. (C) Immunohistochemical staining for TIGIT in SCLC samples with a TIGIT<sup>+</sup> TIL density of 450/mm<sup>2</sup> (left) or 0/mm<sup>2</sup> (right). TIGIT was detected as membranous or cytoplasmic staining in the immune cells. Scale bars, 100  $\mu\text{m}$ . (D) Relation between immune pathway signature and selected gene (*SOX11* and *MYC*) expression in SCLC tumors ( $n = 89$ ). The color scale represents the Spearman correlation coefficient, with the highest value shown in red, median in black, and lowest in green.

**Supplementary Figure S4.** Kaplan-Meier curves for progression-free survival according to *MYC* expression level in the ICI combo-cohort (A) and the chemo-cohort (B). Patients were split into high ( $\geq$ median) and low ( $<$ median) *MYC* expression groups. Abbreviations: CI, confidence interval; HR, hazard ratio.

**Supplementary Figure S5.** Kaplan-Meier curves for progression-free survival according to TMB (A) or predicted frameshift neoantigen load (B) in the chemo-cohort. Patients were split into high ( $\geq$ median) and low ( $<$ median) TMB or neoantigen load groups. Abbreviations: TMB, tumor mutation burden; CI, confidence interval; HR, hazard ratio.

**Figure S1.**

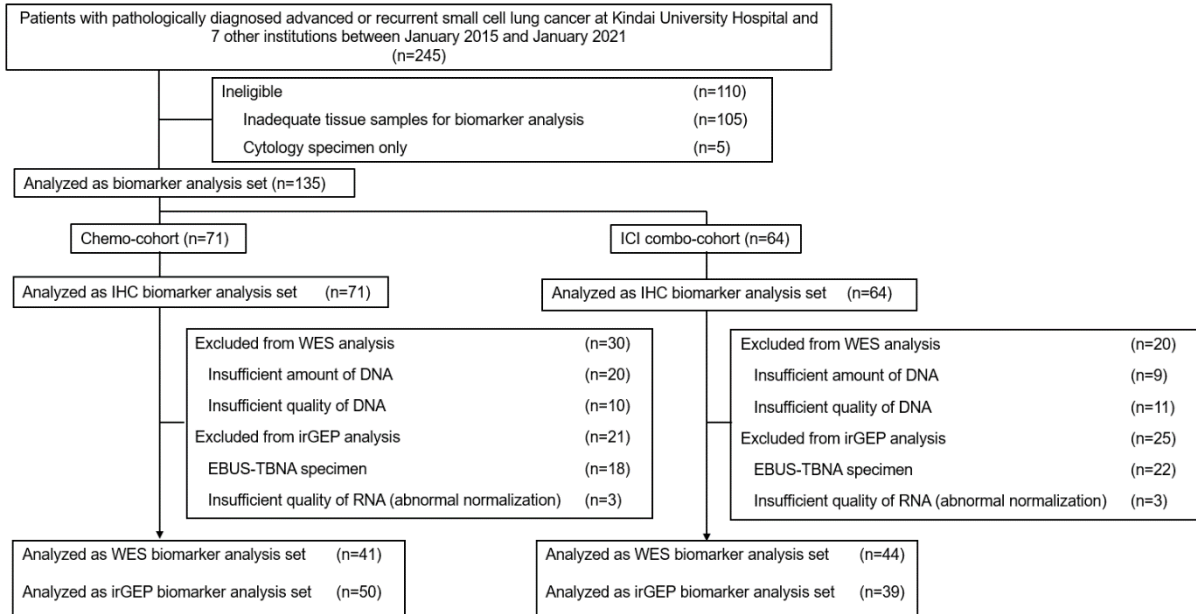


**Figure S2.**

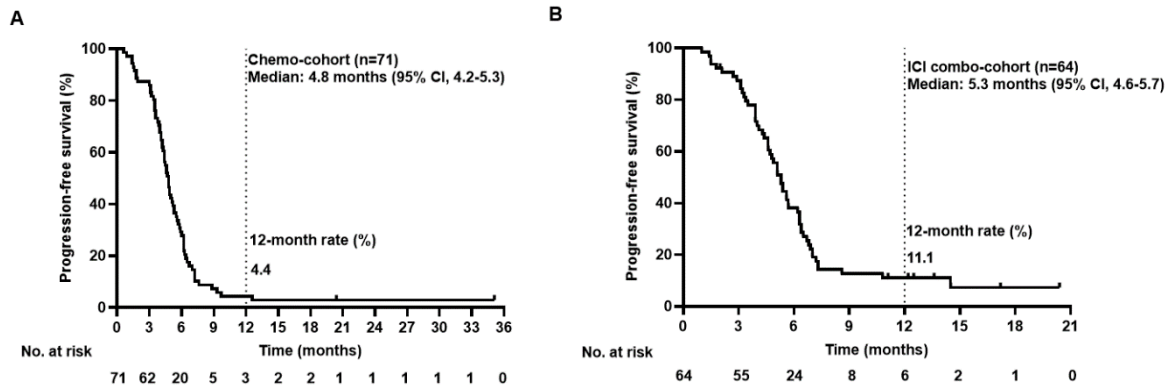


Figure S3.

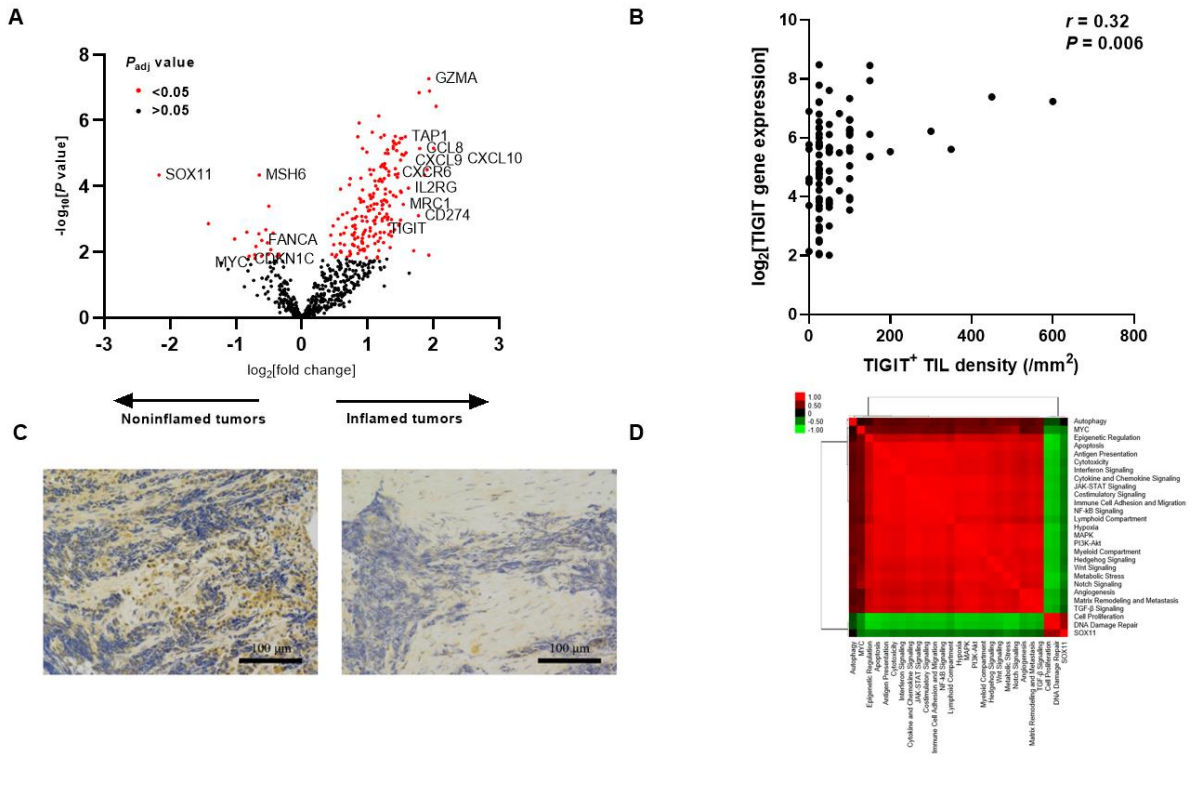


Figure S4.

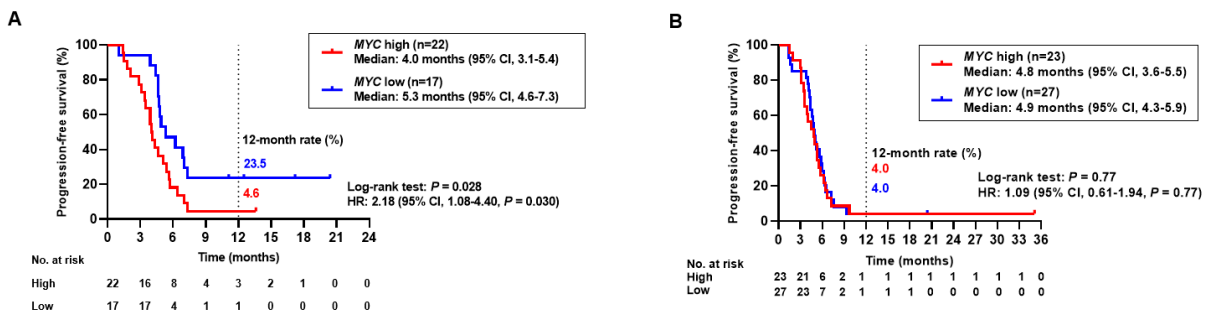
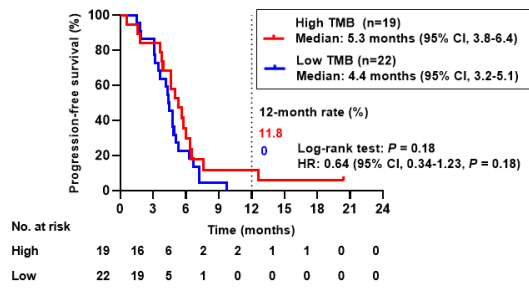
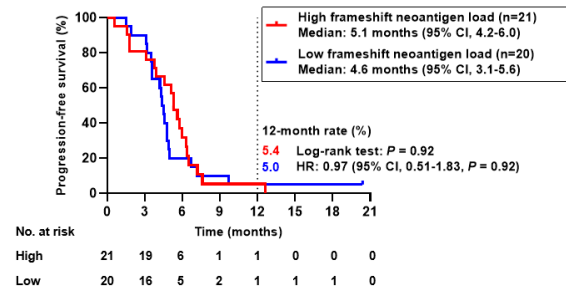


Figure S5.

A



B



**Supplementary Table S1. Characteristics of the Study Patients in the ICI Combo-Cohort According to Tumor Inflammation Status**

Characteristic	Number of patients (%) <sup>a</sup>		<i>P</i> value <sup>b</sup>
	Noninflamed tumors (n=56)	Inflamed tumors (n=7)	
Median age (range), years <sup>c</sup>	72 (34–83)	66 (57–82)	0.369
Sex			
Male	46 (82.1)	7 (100.0)	0.59
Female	10 (17.9)	0 (0)	
ECOG performance status			
0–1	47 (83.9)	7 (100.0)	0.886
2	5 (8.9)	0 (0)	
3–4	4 (7.1)	0 (0)	
Smoking status <sup>d</sup>			
Current or former	56 (100.0)	7 (100.0)	1.00
Never	0 (0)	0 (0)	
Unknown	0 (0)	0 (0)	
Stage			
Limited	3 (5.4)	0 (0)	1.00
Extensive	53 (94.6)	7 (100.0)	
Metastasis at baseline			
CNS	17 (30.4)	3 (42.9)	0.67
Intrathoracic only	7 (12.5)	2 (28.6)	0.260
Extrathoracic	46 (82.1)	5 (71.4)	0.610
Histology			
Small cell	55 (98.2)	5 (71.4)	0.03
Combined	1 (1.8)	2 (28.6)	
Treatment			
Surgery	4 (7.1)	0 (0)	1.00
Radiotherapy	6 (10.7)	0 (0.0)	1.00
Median (range) serum LDH, U/L	257 (145–2143)	242 (8.4–5860)	0.76
Median (range) serum albumin, g/dL	3.5 (2.3–4.3)	3.8 (3.3–4.1)	0.24

Abbreviations: ECOG, Eastern Cooperative Oncology Group; CNS, central nervous system; TPS, tumor proportion score; CPS, combined positive score; NLR, neutrophil-to-lymphocyte ratio; LDH, lactate dehydrogenase.

<sup>a</sup>Percentages may not add up to 100 because of rounding.

<sup>b</sup>*P* values were determined with the Wilcoxon rank sum test or Fisher’s exact test as appropriate.

<sup>c</sup>At the start of treatment.

<sup>d</sup>Current smokers, individuals who had smoked a cigarette within the previous year; former smokers, those who had smoked  $\geq 100$  cigarettes but had quit  $>1$  year before diagnosis; never-smokers, those who had smoked  $<100$  cigarettes.

**Supplementary Table S2. Characteristics of the Study Patients in the Chemo-Cohort According to Tumor Inflammation Status**

Characteristic	Number of patients (%) <sup>a</sup>		<i>P</i> value <sup>b</sup>
	Noninflamed tumors (n=57)	Inflamed tumors (n=13)	
Median age (range), years <sup>c</sup>	73 (35–84)	70 (61–81)	0.839
Sex			
Male	45 (79.0)	9 (69.2)	0.476
Female	12 (21.1)	4 (30.8)	
ECOG performance status			
0–1	45 (78.9)	8 (61.5)	0.473
2	8 (14.0)	4 (30.8)	
3–4	4 (7.0)	1 (7.7)	
Smoking status <sup>d</sup>			
Current or former	55 (96.5)	12 (92.3)	0.36
Never	1 (1.8)	1 (7.7)	
Unknown	1 (1.8)	0 (0)	
Stage			
Limited	7 (12.3)	1 (7.7)	1.00
Extensive	50 (87.7)	12 (92.3)	
Metastasis at baseline			
CNS	9 (15.8)	7 (53.8)	0.007
Intrathoracic only	9 (15.8)	0 (0)	0.193
Extrathoracic	41 (71.9)	12 (92.3)	0.165
Histology			
Small cell	53 (93.0)	12 (92.3)	1.00
Combined	4 (7.0)	1 (7.7)	
Treatment			
Surgery	7 (12.3)	2 (15.4)	0.67
Radiotherapy	4 (7.0)	0 (0.0)	1.00
Median (range) serum LDH, U/L	267 (133–998)	321 (212–1164)	0.334
Median (range) serum albumin, g/dL	3.7 (1.8–4.5)	3.4 (3.0–4.5)	0.344

Abbreviations: ECOG, Eastern Cooperative Oncology Group; CNS, central nervous system; TPS, tumor proportion score; CPS, combined positive score; NLR, neutrophil-to-lymphocyte ratio; LDH, lactate dehydrogenase.

<sup>a</sup>Percentages may not add up to 100 because of rounding.

<sup>b</sup>*P* values were determined with the Wilcoxon rank sum test or Fisher’s exact test as appropriate.

<sup>c</sup>At the start of treatment.

<sup>d</sup>Current smokers, individuals who had smoked a cigarette within the previous year; former smokers, those who had smoked  $\geq 100$  cigarettes but had quit  $>1$  year before diagnosis; never-smokers, those who had smoked  $<100$  cigarettes.